Aging Behavior of PEEK, PTFE, and PI Insulation Materials Under Thermal Oxidative and Humid Conditions for Aerospace Applications

Ahmad, Jawad; Niasar, Mohamad Ghaffarian

DOI
10.1002/app.56858

Publication date
2025

Document Version
Final published version

Published in
Journal of Applied Polymer Science

Citation (APA)
Ahmad, J., & Niasar, M. G. (2025). Aging Behavior of PEEK, PTFE, and PI Insulation Materials Under Thermal Oxidative and Humid Conditions for Aerospace Applications. *Journal of Applied Polymer Science*, *142*(19), Article e56858. https://doi.org/10.1002/app.56858

Journal of Applied Polymer Science

WILEY

Applied Polymer SCIENCE

RESEARCH ARTICLE OPEN ACCESS

Aging Behavior of PEEK, PTFE, and PI Insulation Materials Under Thermal Oxidative and Humid Conditions for Aerospace Applications

Jawad Ahmad | Mohamad Ghaffarian Niasar

Delft University of Technology, Delft, the Netherlands

Correspondence: Jawad Ahmad (j.ahmad@tudelft.nl)

Received: 29 October 2024 | **Revised:** 13 January 2025 | **Accepted:** 30 January 2025

Funding: This work was supported by Dutch Nationaal Groeifonds (NGF) (Grant No. 31194660).

ABSTRACT

Polyether ether ketone (PEEK), polytetrafluoroethylene (PTFE), and polyimide (PI) are widely used in aerospace due to their excellent properties. Understanding their aging behavior is essential for long-term performance in extreme environments. This study examines the effects of thermal oxidative aging (at 250°C over varying periods) under humid conditions on their chemical, structural, thermal, mechanical, and dielectric properties. In PEEK, aging led to solidification and crosslinking phenomenon which resulted in increased tensile strength and storage modulus, while elongation at break and tanδ decreased. Dielectric permittivity, polarization charge density, and leakage current also declined with aging, while AC breakdown strength increased by 1.6% in PEEK. PTFE exhibited surface oxidation, thermal degradation, and a decrease in storage modulus, with an increase in loss tangent. Breakdown strength slightly decreased, while dielectric loss and leakage current increased over aging time. PI underwent severe mechanical degradation, with tensile strength reduced by 54% and elongation by 16%, along with oxidation-induced discoloration. Low-mass polar molecules generated in PI during thermal degradation which contributed to the deterioration of its dielectric properties, lead to increased permittivity, polarization, leakage current, and a lower breakdown strength observed after aging. These findings provide insights into degradation mechanisms, aiding aerospace material selection for extreme environments.

1 | Introduction

With the aim of limiting fuel consumption, the aeronautical market is increasingly moving toward the electrification of propulsion systems, either through electric hybridization of aircraft engines or through a totally electric propulsion system for smaller aircrafts. A significant increase in onboard electrical power management is expected under these conditions, with the electrical distribution and transport system calling on voltage and current levels unheard of in the aeronautical industry. The initial architectures envisaged for hybrid aircraft propulsion systems, for example, require voltage levels of around 1 kV for power levels of up to 500 kVA.

The insulating materials used in aeronautics are governed by current standards. Several polymer materials meet these standards due to advantages like flexibility, low manufacturing costs, and excellent dielectric properties. Aircraft insulation materials in cabling systems basically include polytetrafluoroethylene (PTFE), ethylene tetrafluoroethylene (ETFE), fluorinated ethylene propylene (FEP), polyether ether ketone (PEEK), perfluoroalkoxy (PFA), and polyimide (PI) [1, 2]. PEEK, a high-performance engineering material, offers high strength, modulus, insulation stability, fracture toughness, and dimensional stability. It has recently found wide applications in aerospace, automotive, and nuclear cable industries. PTFE has been used as aircraft wiring insulation since the 1970s and more extensively since 1990 [3]. Its C—F bonds give

it excellent electrical properties, low surface energy, and chemical resistance [4–8]. For air and spacecraft applications, understanding its dielectric response to thermal exposure is important due to the extreme operating temperatures. PIs exhibit impressive chemical and thermal stability. However, PIs are seldom used in modern aircraft due to their rapid degradation under combined exposure to moisture, heat, and mechanical stress [1, 9].

The aging and degradation of insulation materials is a complex process influenced by a combination of internal and external factors [10–13]. There are several external environmental factors that affect the cabling system during the service operation of aircraft. During the service operation of aircraft, a wide range of operating conditions is applicable, for example, temperature ranges from −85°C to 300°C, pressure ranges from 1 to 0.2 atm, a wide range of humidity, combined with an environment with a lot of vibrations. Among the factors which causes the insulation degradation of aircraft cabling system, thermal aging is the primary factor causing material property degradation and potential failure.

Several studies have been done on the aging degradation of cable insulating material. Researchers have studied the phenomenon of crosslinking and thermal degradation reactions occurred under different conditions of heat treatment which is related mainly to the thermal degradation stability of PEEK [14–16]. Danyu et al. [17] studied the influence of thermal oxidative aging on the insulation properties and crystallization behavior of PEEK. The results showed decrease in mechanical, thermal, and insulation properties of PEEK. Similarly, X. Huang et al. [18] have studied the thermal aging of PTFE in the fluid state that resulted in the deterioration of its electrical insulating performance. S. W. Li et al. [19] studied the effect of thermal aging on electrical and mechanical properties of PTFE. It was observed that the relative permittivity of PTFE decreased as a result of aging. Although extensive research has been conducted on the dielectric properties of PI materials [20–22], investigations into the influence of thermal aging on dielectric performance remain limited, with existing findings often exhibiting uncertainty and inconsistency. In addition, researchers have studied the negative effects of moisture absorption (absorbing up to 3 wt.% of water from atmospheric humidity) in PI which limits its dielectric properties. It has been observed that absorbed water is associated with increased dielectric permittivity, decreased electrical resistivity, and potential mechanical failures such as cracks, delamination, and loss of adhesion [23–26]. Although studies concerning the aging under environmental conditions, for example, heat and humidity have been done for the materials (PEEK, PTFE, and PI) used in cable insulation, there are very few studies that presents a comprehensive investigation on the combined effect of thermal oxidative aging with humidity on the physiochemical and insulating properties of these materials in aircraft operational environment. So, it is important to study the degradation behavior of these material (PEEK, PTFE, PI) under thermal aging and humidity.

This research presents a comprehensive study of the effect of thermal oxidative aging and humidity on the degradation behavior of PEEK, PTFE, and PI materials for the service evaluation of their usage as insulation materials for aircraft cabling system. The influence of thermal oxidative aging with humidity on the structure and properties (chemical and physical structure morphology, optical properties, thermal properties, mechanical, and insulating properties) of PEEK, PTFE, and PI, is studied. The experimental results could be a practical reference in relevant fields of research and may offer valuable guidance for design considerations and production of PEEK, PTFE, and PI materials for future engineering applications.

2 | Experimental and Methodologies

2.1 | Materials

PEEK and PI materials in the form of films were obtained from Shenzhen Jinyuanbao Plastics Materials Co. Ltd. PTFE films were received from Shanghai Daoguan Rubber & Plastics Co. Ltd. The thickness and width of these film are 0.1 mm and 50 mm, respectively. The molecular structures of PEEK, PTFE, and PI provided by the companies are shown in Figure 1. The relative permittivity of PEEK, PTFE, and PI at room temperature is 3.9, 2.1, and 3.2, respectively.

2.2 | Thermal Oxidative Aging With Humidity

The films of PEEK, PTFE, and PI with 0.1 mm thickness were cut first in dimensions of 50 × 200 mm (width × length). The samples were attached to the wire mesh shelves of the oven as shown in Figure 2. A minimum distance of 5 cm between samples and the oven walls were maintained to avoid contact and ensure smooth airflow between samples (Figure 2). The wire mesh shelves were then inserted into the oven set at 250°C for thermal oxidative aging. The aging profile is highlighted in Figure 3. After a thermal oxidative stress of 20 h, the oven temperature was reduced to 90°C and the samples were subjected to a humidity shower of 3 h at 90% relative humidity (RH). The RH% was provided and maintained by the chamber, ensuring precise control of humidity levels throughout the aging period. After the humidity exposure, the oven temperature was raised to 250°C again and the thermal oxidative stress continued as shown in Figure 3.

During aging, samples were collected from oven at intervals (24 h, 72 h, 120 h, 170 h) and allowed to cool down in ambient

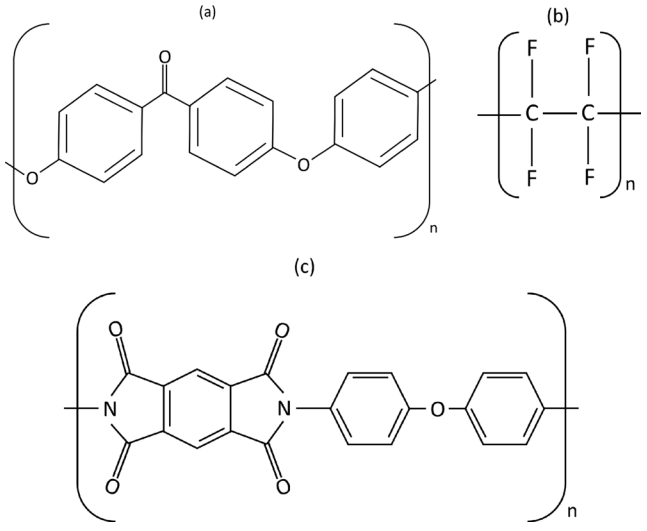

FIGURE 1 | Chemical structures of (a) PEEK, (b) PTFE, and (c) PI. [Color figure can be viewed at wileyonlinelibrary.com]

conditions which are finally subjected to testing. The surface temperature range read by IR thermometer during collection of samples from oven was between 200°C and 235°C.

2.3 | Fourier Transformed Infrared (FTIR) Spectroscopy

FTIR spectra were recorded in the range of 4000–400 cm^{-1} using a Nicolet iS50 FTIR (Thermo Fisher Scientific, USA) in transmittance mode. The resolution was set to 4 cm^{-1}, with each spectrum representing the average of 30 scans. Atmospheric background spectra were measured and automatically subtracted from the sample spectra.

2.4 | Microscopic Morphology

SEM was performed using SU8600, Hitachi, Japan coupled with energy dispersive spectrometer (EDS) Ultim Max 170 provided by Oxford Instruments, UK to obtain microstructure morphology and elemental composition data of the surface and cross-section of PEEK, PTFE, and PI films. The samples were coated with gold to limit charging effect and are subjected to a voltage of 10 kV. A polarized optical microscope namely Olympus BX53 with DP-26 digital camera is also used to study the optical morphology. Samples are placed between two polarizing filters (crossed) for careful objective observation.

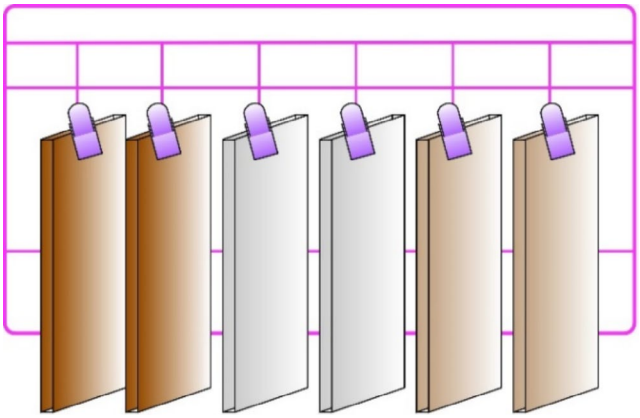

FIGURE 2 | Illustration of samples attachment to aging oven mesh tray. [Color figure can be viewed at wileyonlinelibrary.com]

2.5 | Mechanical Properties

The samples were cut in dumbbell shape and the tensile strength (MPa) and elongation (%) are tested. The test is completed at ambient atmospheric conditions with a tensile rate of 15–20 mm/min. Five specimens of each sample type are tested consecutively and measurements are taken and average is calculated with error. Dynamic mechanical analysis (DMA) was also performed at a frequency of 1 Hz using a TA Q800 analyzer to investigate the molecular dynamics of samples.

2.6 | Differential Scanning Calorimetry (DSC) and Thermogravimetric Analysis (TGA) Analysis

DSC and TGA was done using DSC/TGA equipment provided by Mettler-Toledo, Switzerland. A sample weighing in a range of 20–30 mg is heated at a heating rate of 20°C/min in inert environment (N_2) from room temperature to 700°C to obtain DSC and TGA curves. The crystallinity (X_c) of aging sample is calculated according to the formula.

$$X_c = \frac{\Delta H_m}{\Delta H_{m^o}} \times 100\,\% \tag{1}$$

where ΔH_m corresponds to the enthalpy of melting and ΔH_{m^o} defines the melting enthalpy of fully crystallized PEEK taken as 130 J/g [17].

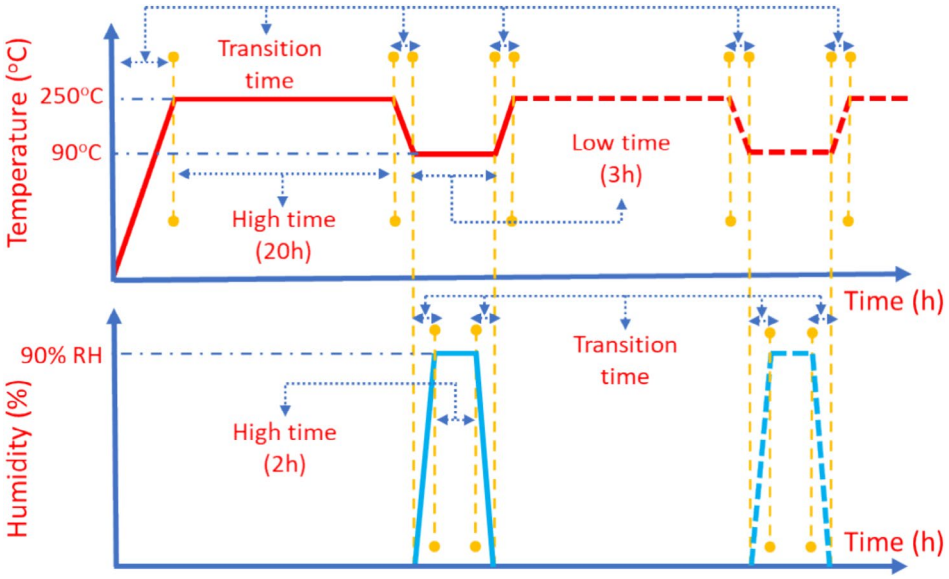

FIGURE 3 | Temperature and humidity profile for aging. [Color figure can be viewed at wileyonlinelibrary.com]

2.7 | Optical Properties

Optical UV–vis spectra of samples is measured using full wavelength UV–Vis–NIR spectrometer LAMBDA 1050+, provided by PerkinElmer, UK. The spectra is measured at ambient conditions in a wavelength range of 200–800 cm^{-1}.

2.8 | Dielectric Properties

Dielectric properties including relative permittivity, dielectric loss ($\tan\delta$), polarization charge density, leakage current density, and AC breakdown strength are recorded. Relative permittivity and dielectric loss were measured using a Novocontrol Concept 80 broadband dielectric analyzer at room temperature, covering a frequency range from 10^{-1} to 10^{6} Hz. The relative permittivity of samples was also recorded with the frequency of 50 Hz over a broad temperature range from 25°C to 200°C with a heating rate of 1°C/min using multi-frequency LCR meter (E4980AL). The polarization charge density and leakage current density measurements were acquired via a ferroelectric tester system (PolyK, USA) using an ion sputtering instrument to spray gold on the sample, with an effective polarization area of 3.14 mm^2. The polarization charge density and leakage current density were measured at (25°C and 200°C) and (50 MV/m and 100 MV/m), respectively. For AC breakdown strength measurement, samples are prepared into a circular form with an optimal diameter and subjected to testing using an AC dielectric strength tester. The dielectric breakdown strength is recorded, and five measurements are performed to determine the average value.

3 | Results and Discussion

3.1 | PEEK

3.1.1 | FTIR Analysis

The change in the chemical composition of PEEK with aging time captured in region (2000–600 cm^{-1}) is highlighted in Figure 4. FTIR spectra shows the characteristic peak at 1650 cm^{-1}, which is related to the aromatic stretching vibration of carbonyl group (CO bond). Characteristic peaks at 1597, 1410, and 1489 cm^{-1} indicate the aromatic skeletal vibration of phenyl rings (Φ). The asymmetric stretching vibration bands of the diphenyl ether group were observed at 1280, 1220, and 1185 cm^{-1}. Peaks at 1151 and 1096 cm^{-1} are associated with the deformation bands of aromatic hydrogen in-plane. Afterward, the peak at 1310 cm^{-1} can be ascribed to the bending motion of C—C and (=O)—C groups [27]. Peak at 923 cm^{-1} is attributed due to aromatic out plane bending [28]. Peaks at 769, 864, and 832 cm^{-1} are out-of-plane bending modes of the aromatic hydrogen (C—H in aromatic ring). The stretching vibrations at 1160 and 1010 cm^{-1} correspond to Φ—O or Φ—CO stretching vibrations. The changes in the 1280/1310 cm^{-1} intensity ratios are indicative of changes in the crystallinity of PEEK [29, 30], and the variations around 1110 cm^{-1} show crosslinking mechanisms take place [31, 32]. Lastly, the decrease in the aromatic C—H peaks around 835, 766, and 673 cm^{-1} indicates the damage of molecular chains and possible occurrence of surface carbonization observed in the aged samples of PEEK [33, 34].

Under different aging durations, no new absorption peaks appeared in the PEEK IR spectra, and the positions of the characteristic peaks remained unchanged, indicating that no new functional groups were formed. However, the peak intensities did change. The relative crystallinity (R_C) of PEEK samples at different aging times can be calculated using Equation (2), as outlined in the literature [35].

$$R_c = \frac{A_{1280}}{A_{1310}} \times 100\% \tag{2}$$

where A_{1280} represents the peak area of 1280 cm^{-1} (corresponding to the diphenyl ether group), and A_{1310} represents the peak area of 1310 cm^{-1} (corresponding to the C—C and (=O)—C groups). Figure 4b demonstrates that the ratio of the 1280 cm^{-1} and 1310 cm^{-1} bands decreases quickly during the initial phase of the aging process, followed by a slower decrease at later stages. This behavior is attributed to oxidation of the sample surface, which is faster in the early stages, resulting in a sharp reduction in relative crystallinity. As aging progresses, the rate of material oxidation stabilizes, and the combined influence of potential crosslinking structures and thermal oxidative aging leads to a gradual decline

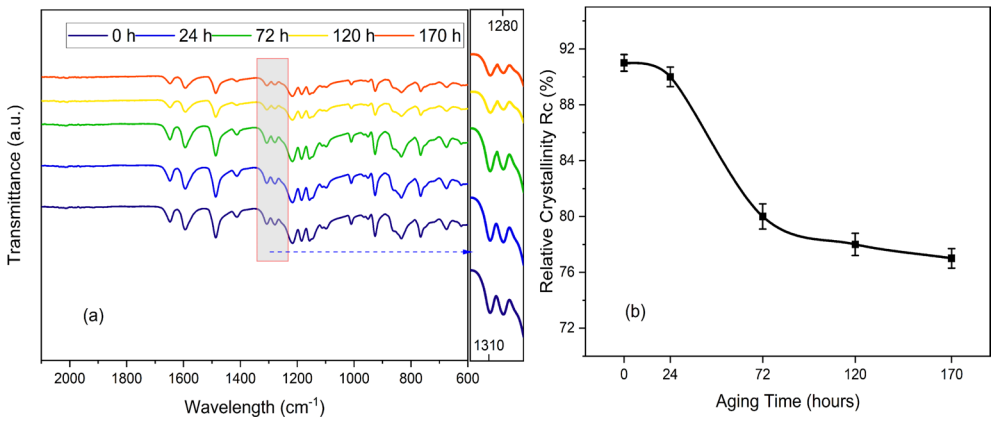

FIGURE 4 | (a) FTIR spectra of PEEK samples with aging time; (b) R_c variation with aging time. [Color figure can be viewed at wileyonlinelibrary.com]

in the relative crystallinity (R_c) of the PEEK samples. It is worthy to say that the aging in PEEK is mainly dominated by thermal oxidative stress.

3.1.2 | Microscopic Morphology

Surface SEM results highlighted in Figure 5 show that thermally affected regions appear sporadically on the surface of aged PEEK samples in small areas. The surface of pristine PEEK appeared smooth however, aged samples have adopted a rough appearance with aging progress. Surface roughness and some local heterogeneities, identifiable as microvoids or pits, for example, some holes also appear suggesting thermal degradation and potential embrittlement which can be attributed to oxidative fracture and surface carbonization of PEEK polymer. The phenomenon is observed in FTIR results that detected the possible occurrence of surface carbonization.

The main chemical components highlighted using EDS mapping in Figure 6 show an increase in carbon content and reduction in oxygen content. This suggests that the oxidative degradation process may have led to preferential loss of oxygen-containing volatile by-products (mainly CO_2, CO), leaving a carbon-rich surface layer. The surface EDS elemental data are also enlisted in Table 1a. It can be seen from results that the carbon forming property of PEEK has increased which is also an indicative of increase in the restricted amorphous region of PEEK.

The cross-sectional SEM micrographs are shown in Figure 7. It can be seen from the results that the aging of PEEK has led to noticeable structural changes, as evidenced by SEM images, and image analysis. Image analysis in Figure 7c,d highlights roughness, defects, and structural heterogeneity. The results indicate more pronounced texture differences across the surface with pits and uneven surface distribution. The rectangular-marked region in Figure 7b highlights the probable depth and localized nature of thermal degradation. In the aged sample, for example, PEEK 170 h, the noticeable degradation can be seen, with a maximum depth measurable from the surface cracks and internal layers. This is consistent with thermal oxidative degradation, which may spread internally over time. The surface irregularity in aged PEEK indicates prominent thermal oxidative degradation, which may lead to loss of mechanical integrity (potential embrittlement can occur). Carbon to oxygen (C:O) ratio slightly increases in the aged sample (from 82.93% to 83.29%), indicating a higher concentration of carbon-rich structures, reflecting carbonization and formation of a brittle surface layer. The cross-sectional SEM EDS results of PEEK in Table 1b are consistent with surface SEM EDS results.

The optical photos from POM in Figure 8 show some pinholes that appeared on the surface of aged PEEK sample. The POM results and visible inspection show reduction in surface gloss of PEEK and increase in surface roughness with aging time. Combining with chemical composition analyses from FTIR of all samples, a reasonable interpretation could be obtained that the appearances of surface defects and degradation is due to the changes of molecular chain that mainly includes the damage of C—H bond of benzene rings and ether bond of main chains and possible carbonization of surface.

3.1.3 | Mechanical Properties

Thermal oxidative aging impacts the mechanical properties such as tensile strength and breaking elongation of polymers. The effect of aging on tensile strength and breaking elongation of PEEK is shown in Figure 9a. Stress and strain curve of PEEK samples are presented in Figure 9b. It can be seen clearly that the tensile strength increases slowly with increase in aging time. In the aging time range (0–170 h), the tensile strength increases 110–114.5 MPa. On the other hand, elongation at break shows reduction with the progress of aging. The breaking elongation reduced 24.5% in aging time frame (0–170 h). The tensile strength and breaking elongation of PEEK are primarily related to their

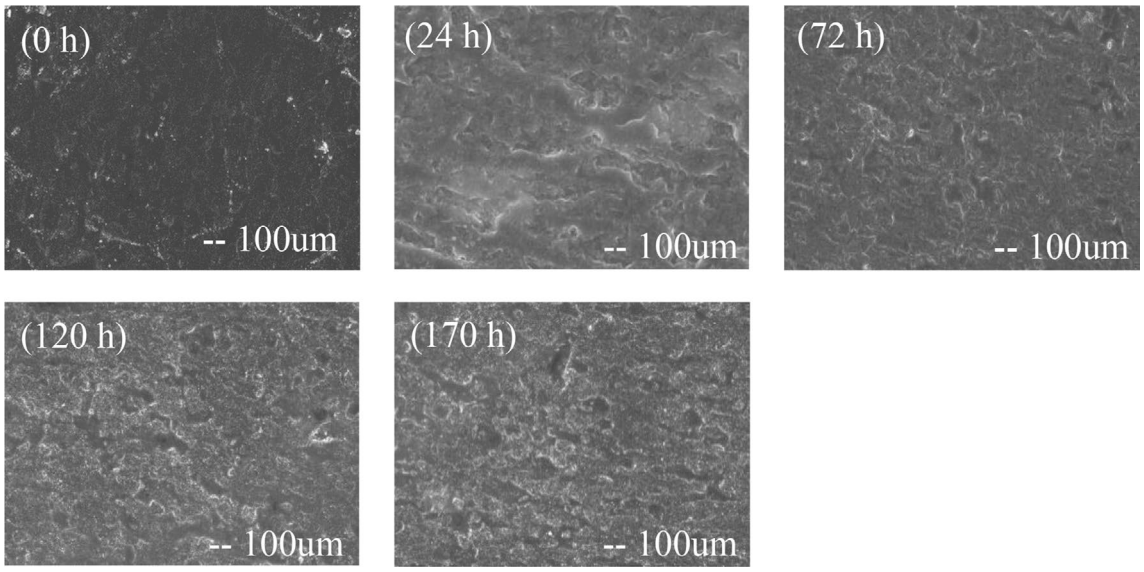

FIGURE 5 | Surface SEM of PEEK samples with aging time.

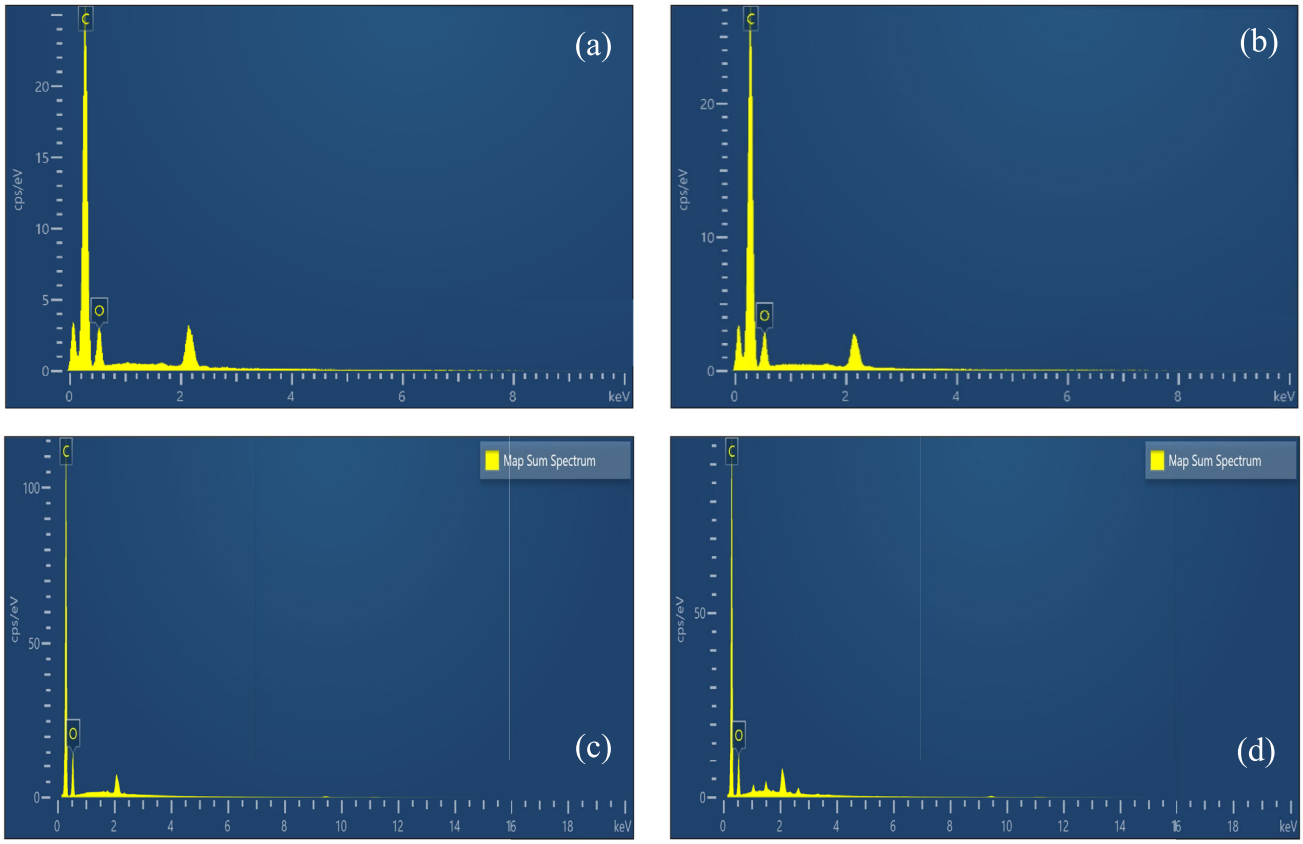

FIGURE 6 | EDS elemental scan of PEEK samples: (a) fresh (surface), (b) aged 170 h (surface), (c) fresh (cross-section), and (d) aged 170 h (cross-section). [Color figure can be viewed at wileyonlinelibrary.com]

TABLE 1A | EDS surface scan data of PEEK samples.

	EDS elemental weight (%)		Weight (%) sigma	
Elements	**PEEK (0 h)**	**PEEK (170 h)**	**PEEK (0 h)**	**PEEK (170 h)**
C	78.89	81.35	2.28	0.36
O	19.97	18.65	0.68	0.36

TABLE 1B | EDS cross-section scan data of PEEK samples.

	EDS elemental weight (%)		Weight (%) sigma	
Elements/ ratio	**PEEK (0 h)**	**PEEK (170 h)**	**PEEK (0 h)**	**PEEK (170 h)**
C	82.93	83.29	0.10	0.11
O	17.07	16.71	0.10	0.11
C:O ratio (atomic)	6.47	6.64		

crystalline structure. Considering semi-crystalline polymers like PEEK, the material mainly consists of crystalline, amorphous, and restricted amorphous regions [36]. During the initial phase of thermal aging process, the molecular chains in both amorphous and crystalline regions begin to degrade. This leads to a more ordered state in the amorphous regions, while the restricted amorphous regions increase under high-stress conditions. As thermal aging progresses, preferential crosslinking might have occurred in these high-stress amorphous regions, resulting in an increase in tensile strength and a reduction in breaking elongation [17]. The results are indicative of increase in brittleness and hardness of PEEK during aging process.

The variation of DMA storage modulus and tan δ of PEEK samples as a function of temperature is shown in Figure 9c and Figure 9d, respectively. Figure 9d indicates that the glass transition temperature (T_g) of PEEK, defined as the temperature at the peak of tan δ, occurs at 153.4°C, corresponding to (α) relaxation that closely aligns with the previously reported value [37]. The storage modulus for all PEEK samples exhibits a gradual and progressive decline with increasing temperature, with a notable reduction observed in the temperature range of 140°C–200°C, corresponding to the material's glass transition. This decrease in modulus is attributed to energy dissipation processes associated with the cooperative movements of polymer chains [38]. It is also evident from DMA results that the storage modulus of PEEK shows a slight increase with aging time (0–170 h) in the lower-temperature region (below T_g). The curves gradually converge and decrease at higher temperatures near and beyond T_g. The increase in storage modulus in aged samples of PEEK unveils the increased load-carrying capacity and visco-elastic stiffness increasing mechanism of polymer [39]. Thermal oxidative

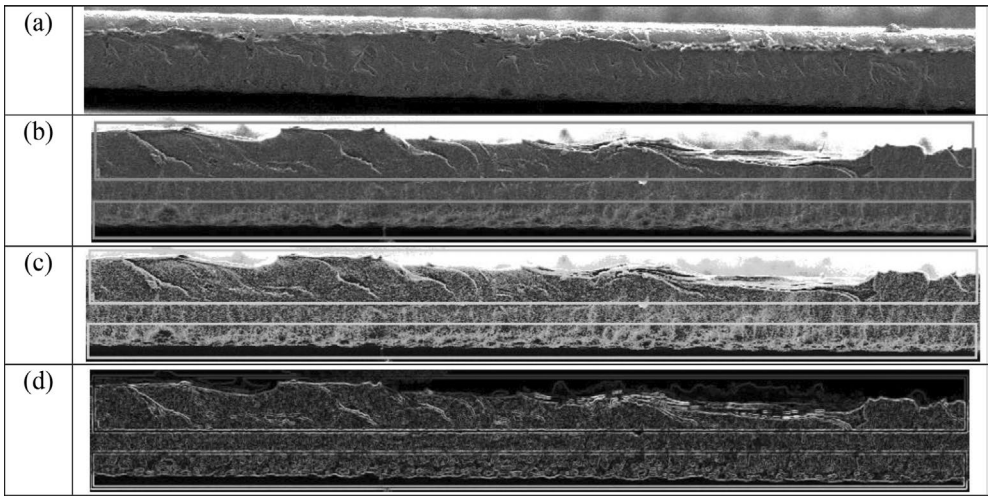

FIGURE 7 | Cross-sectional SEM of PEEK samples: (a) PEEK 0 h, (b) PEEK 170 h, (c) high contrast PEEK 170 h, and (d) Sobel edge detection PEEK 170 h.

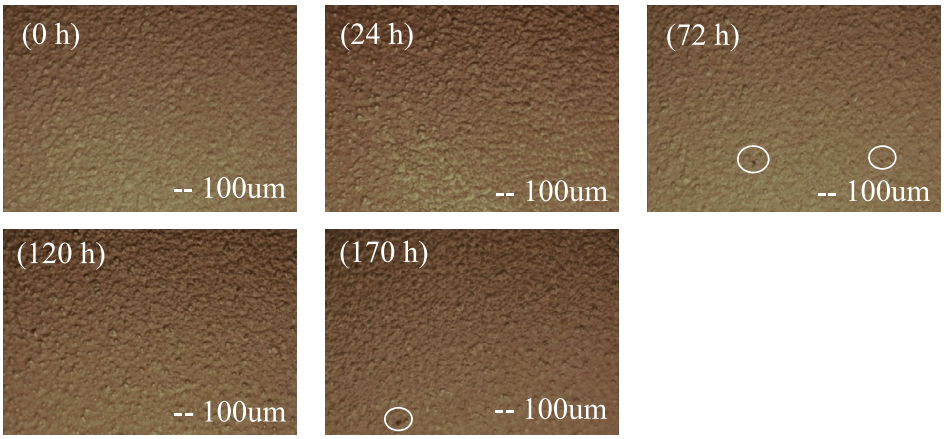

FIGURE 8 | POM of PEEK samples with aging time. [Color figure can be viewed at wileyonlinelibrary.com]

aging may have resulted crosslinking in the amorphous regions of PEEK, leading to increased stiffness at lower temperatures. This restricts molecular mobility, causing a higher storage modulus in the glassy region. Moreover, the softening of the material is dominated by the relaxation of amorphous chains around T_g. Crosslinking in these regions delays and mitigates this transition slightly, as reflected in the smaller modulus drop.

The tan δ of materials reflects the balance between the viscous and elastic phases in polymer-based systems. The tan δ (damping peak), typically observed in the glass transition region, is associated with the motion of side groups, low molecular weight units, or molecular chains in the polymer. A higher damping peak indicates greater molecular mobility [40]. It can be seen from Figure 9d that the tan δ peak (α-relaxation) of PEEK decreases in height and shifts toward higher temperatures (153.4°C–156.0°C) with aging (from 0 to 170 h). The relaxation process is highly sensitive to molecular dynamics and the state of the amorphous regions. Crosslinking in PEEK reduces the intensity of relaxation peak (tan δ), as the crosslinked regions restrict chain movement [41]. As aging progresses, oxidation and crosslinking stiffen the amorphous regions in PEEK, and reduces the segmental motion of the amorphous chains, requiring more thermal energy to achieve the glass transition. The broadness of the peak in tan δ curves also appears to increase slightly with aging which suggests increased heterogeneity in the amorphous regions of PEEK caused by crosslinking, which creates a range of relaxation times.

The increased storage modulus and reduced tan δ peak as a result of aging of PEEK indicate enhanced rigidity and reduced damping, making the PEEK more resistant to deformation under mechanical stress. However, the reduced damping capacity may increase brittleness in PEEK as observed in study of mechanical properties.

3.1.4 | DSC and TGA Analysis

TGA was used to study the thermal stability of PEEK samples when subjected to aging. The thermal weight loss curves are drawn in Figure 10a, and the TGA characteristic parameters including the initial decomposition temperature at 5% weight loss ($T_{5\%}$), maximum decomposition temperature (T_{max}), and residual weight

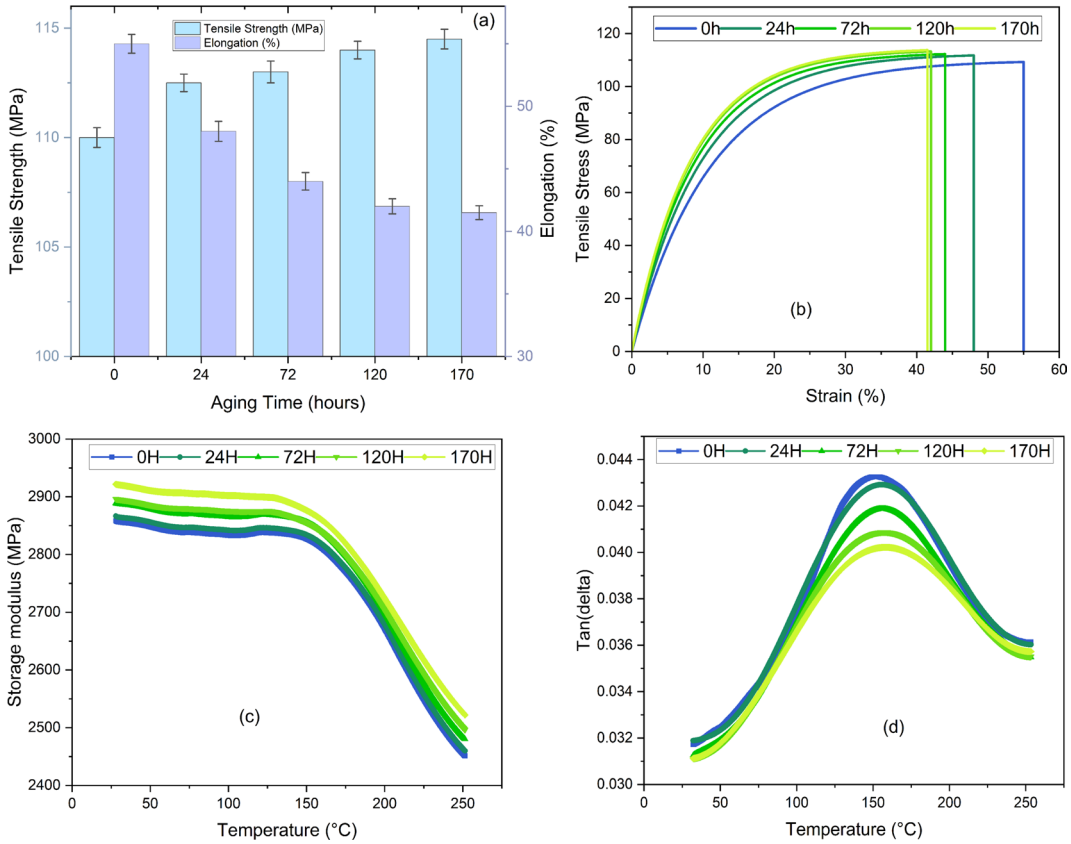

FIGURE 9 | Mechanical properties of PEEK samples with (a) aging time, tensile stress, and elongation, (b) stress versus strain curves, (c) DMA storage modulus versus temperature, and (d) DMA tan δ versus temperature. [Color figure can be viewed at wileyonlinelibrary.com]

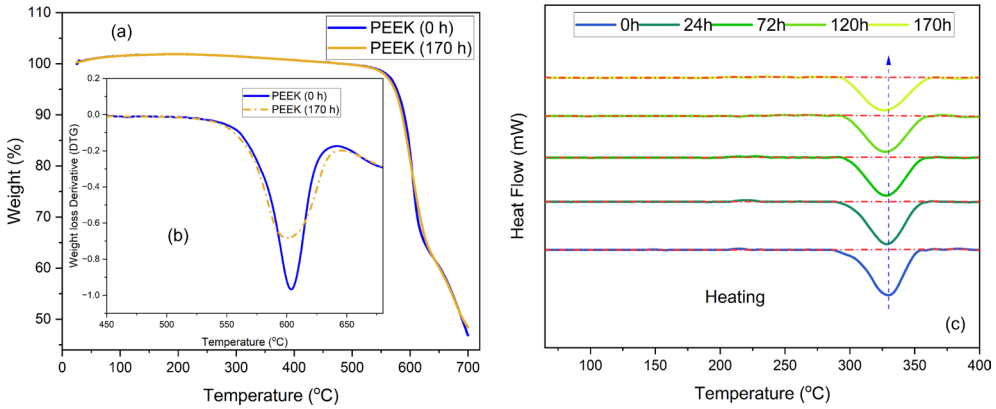

FIGURE 10 | Thermal analysis curves of PEEK samples: (a) TGA, (b) DTG, and (c) DSC. [Color figure can be viewed at wileyonlinelibrary.com]

percentage hereby defined as carbon residue rate (R_w) are listed in Table 2. These are important parameters to assess the thermal stability of polymers. The characteristic TGA curve of PEEK fresh and aged sample is shown in Figure 10a. Rapid and substantial weight loss observed from 500°C to 650°C. During thermal decomposition of PEEK, by-products observed were mainly CO and CO_2 with a few phenolic decomposition products has been reported [42–44].

TABLE 2 | TGA and DTG data of PEEK samples.

Aging time (h)	$T_{5\%}$ (°C)	T_{max}	R_w
0	576.8	602.2	46.8
170	573.2	600.6	48.4

It can be seen from TGA curve that the initial decomposition temperature of PEEK has decreased due to aging and the carbon residue yield (R_w) of the PEEK has increased from 46.8% to 48.4%, which is indicative of the carbonization of PEEK material. The derivative thermogravimetric (DTG) curve shown in Figure 10b and the corresponding data listed in Table 2 show that the maximum decomposition temperature of PEEK has decreased as a result of aging. This is attributed to the enhancement of thermal oxidative aging at higher temperature which causes degradation reaction to occur inside PEEK. As a result, the thermal stability of PEEK reduces due to destruction of molecular chain at higher temperature [45, 46].

In order to study the effect of aging on the crystalline and melting behavior of PEEK, DSC test was performed. The DSC heating curve is shown in Figure 10c. The parameters of DSC curve, maximum melting temperature (T_p), peak area (ΔH_m), and test crystallinity (X_c) obtained from analysis are listed in Table 3. The test crystallinity X_c of PEEK samples was calculated using Equation (1). The thermal properties reflected from DSC endothermic melting peak observed around 320°C–350°C in PEEK samples indicate that the thermal aging does not exert significant influences on the melting and crystallinity of PEEK. However, a reduction in melting point and crystallinity is observed. The peak area ΔH_m also decreases as a result of thermal aging of PEEK.

It has been observed that the melting point of a polymer crystal is affected by lamellar thickness during the process of polymer crystal change [47]. Therefore, the lamellar thickness of PEEK samples is calculated using Thompson–Gibbs relationship which is given as follows:

$$L = \frac{2\gamma_e}{\Delta H_m^o} \frac{T_m^o}{T_m^o - T_m} \tag{3}$$

where L defines the lamellar thickness, T_m is melting temperature of PEEK polymer crystal, T_m^o is equilibrium melting temperature which is 385°C, ΔH_m^o is 130 J/g, and γ_e is the surface energy of crystal which is 180×10^{-7} J/cm^2. The values of lamellar thickness are listed in Table 3. It is evident from the results that the lamellar thickness has reduced due to aging. During DSC analysis, the heat absorbed by the crystalline material during melting process is entirely utilized to disrupt the crystal lattice structure. The greater the lattice energy, the more heat is usually required to induce melting. So, the decrease in melting point of PEEK as a result of aging indicates that internal molecular chains (mainly aromatic C—H bond as discussed in FTIR and SEM) of PEEK material was destructed and oxidized at high temperature which causes decrease in the Van der Waals force between polymeric chains [14, 48]. The internal crystal structure of the PEEK material was damaged due to degradation and carbonization and the regularity of the whole molecular chain was reduced. This process increases the crystal defects in sample and results in reduction of lamellae thickness, eventually reducing melting point [17].

3.1.5 | Optical UV–Vis Spectrum Analysis

In order to study the influence of aging on the optical properties of PEEK, UV–vis spectrum is recorded. It has been reported that UV–vis can be used as a useful technique to check degradation as a result of aging and can be related to the dielectric and insulating properties of the material [48]. It also highlights the changes in the electronic excitation states between the energy levels of a material. To analyze the changes in electronic excitation states, optical band gap of PEEK samples is calculated based on the following relationship.

$$(\alpha h\nu)^n = B(h\nu - E_g) \tag{4}$$

where α, $h\nu$, n, B, and E_g represent the absorption coefficient, photon energy, nature of electronic transition, proportionality, and optical energy band gap, respectively. The value of band gap can be obtained by extrapolating the linear part of the plot of $(\alpha h\nu)$ with photon energy as shown in Figure 11b.

UV–vis absorption spectra of fresh and aged PEEK samples is highlighted in Figure 11a. It can be seen from spectra that there is no bathochromic or hypsochromic shifts observed as a result of aging. The values of optical band gap reflect no markable changes in the electronic excitation states between energy levels of PEEK due to aging. The virgin PEEK appears glossy brown in color, however the aged samples show no obvious color change. However, reduction in glossiness with increase in roughness is observed in PEEK-aged samples as previously mentioned in SEM results. This could be the reason for a slight increase in the absorption of light in the visible range (400–800 nm) observed in aged samples of PEEK. Since, no noticeable changes were observed in the UV–vis spectra of PEEK, it reflects that the effect of thermal aging on dielectric and insulating properties of PEEK cannot be studied using this technique.

3.1.6 | Dielectric Analysis

The broadband dielectric spectroscopy (BDS) results of PEEK are shown in Figure 12a and Figure 12b. It can be seen from Figure 12a that the dielectric constant of PEEK decreases progressively with aging (0–170 h). The frequency dependency is minimal, suggesting that the primary dielectric relaxation processes are not strongly frequency-dependent in the range measured. The dielectric polarization ability of PEEK is decreased

TABLE 3 | DSC data of PEEK samples.

Aging time (h)	T_p (°C)	ΔH_m (J/g)	X_c (%)	I (nm)
0	330.1	27.0	20.7	22.58
24	328.6	25.5	19.6	21.98
72	328.0	24.3	18.7	21.75
120	327.5	22.5	17.3	21.56
170	327.0	20.7	15.9	21.37

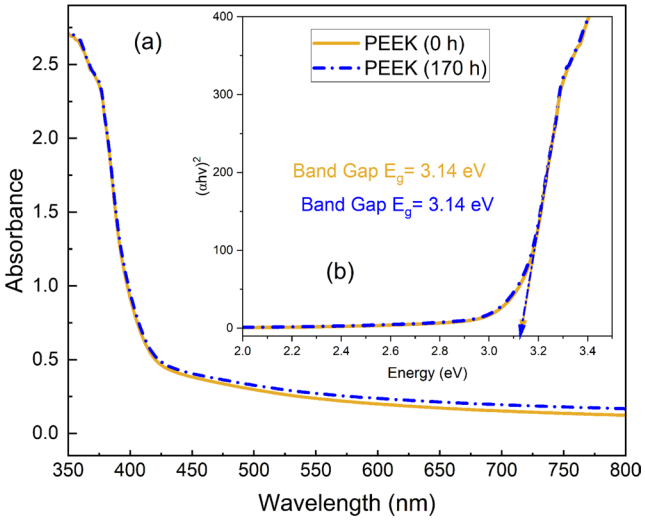

FIGURE 11 | UV–vis spectra of PEEK samples: (a) spectra; (b) Tauc plot. [Color figure can be viewed at wileyonlinelibrary.com]

as a result of aging. The suppression of dielectric polarization in PEEK and diminishing of glass transition observed in DMA results, are closely related to the occurrence of crosslinking in PEEK due to aging. PEEK exhibits two distinct relaxation peaks in its dielectric spectrum as shown in Figure 12b, indicating the presence of two types of bound charges with different characteristic frequencies namely space charge polarization which occurs in the low-frequency range of 10^{-2}–10^{2} Hz and orientational polarization usually observed in the high-frequency range of 10^{5}–10^{10} Hz [49]. Due to the aging process, the relaxation dynamics changes, and the low-frequency relaxation processes are suppressed prominently as evidenced by changes in the frequency response of tan(δ) shown in Figure 12b. At low frequencies (usually 10^{-1}–10 Hz), the energy dissipation is usually considered in terms of conductivity loss and polarization loss which is reduced due to aging. As aging progresses (from 0 to 170 h), the rigid network inside PEEK suppresses low-frequency relaxation processes (space charge polarization is reduced due to restricted carrier movement) thereby reducing dielectric loss. Overall, the BDS results of PEEK indicate that thermal oxidative aging induces crosslinking in PEEK, leading to a reduction in molecular dynamics, lower dielectric constant, and suppressed energy dissipation (tan δ). This behavior is consistent with the formation of a rigid crosslinked network that limits dipolar orientation and relaxation processes. These findings can be correlated to the material's enhanced mechanical stability (rigidity) but reduced flexibility due to aging as observed in the analysis of mechanical properties.

The variation of dielectric permittivity of PEEK with temperature is shown in Figure 12c. It can be seen that the dielectric permittivity decreases as a result of increase in temperature. Also, a reduction in dielectric permittivity of PEEK is recorded as a result of aging. The dielectric constant of PEEK reduces from 3.9 to 3.1 with the progress of aging (0–170 h) measured at room temperature. A similar decrease is recorded at high temperature, for example, at 200°C.

In order to access the change in dielectric permittivity of PEEK with temperature and aging, the polarization charge density of samples is measured at 20°C and 200°C and shown in Figure 13. It can be seen that the polarization charge density of PEEK samples reduces when temperature is increased from 20°C to 200°C. Also, the polarization charge density is reduced in PEEK as a result of aging. This shows that the resultant charge accumulation become difficult and the polarization ability is reduced in PEEK as result of aging especially at high temperature. With the progress of aging, crosslinked structure may appear in PEEK that will restrict orientation and relaxation of dipoles, thereby reducing the polarization ability of PEEK. At a later stage of aging, PEEK solidified and carbonized which may result in tight chain arrangement which may have further limited the polarization inside PEEK. Thinking of the conventional polymers where dielectric permittivity increase as a result of aging [50–52], the reduction in dielectric constant in this research is a bit odd. However, similar results of decrease in dielectric permittivity have been reported already in the literature [48, 53].

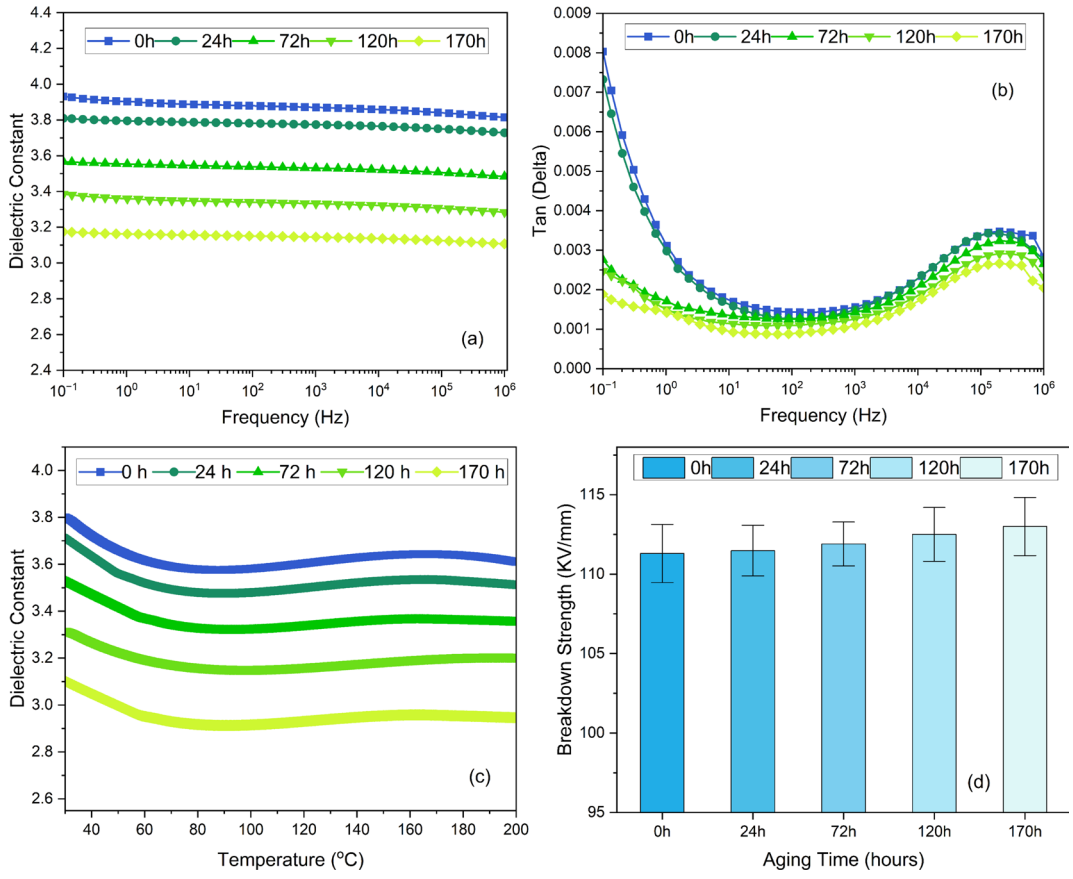

FIGURE 12 | Dielectric properties of PEEK samples with aging time: (a) dielectric constant, (b) dielectric loss, (c) dielectric constant versus temperature, and (d) AC breakdown strength. [Color figure can be viewed at wileyonlinelibrary.com]

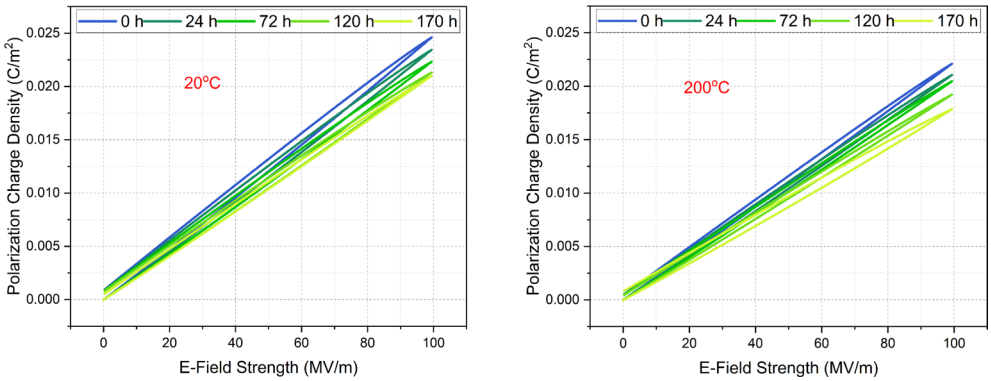

FIGURE 13 | Polarization of PEEK samples with aging time at room temperature and 200°C. [Color figure can be viewed at wileyonlinelibrary.com]

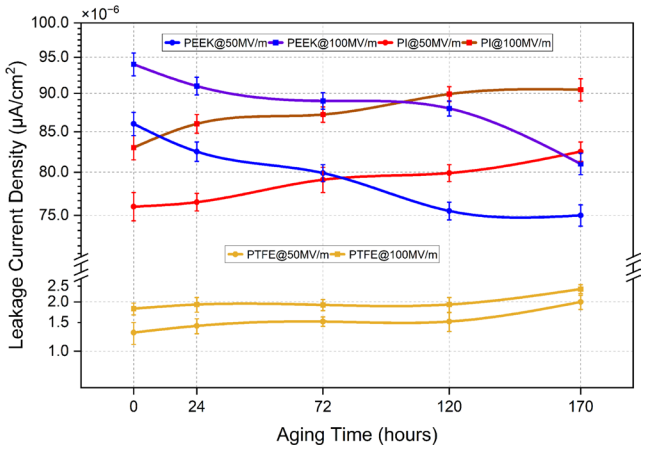

FIGURE 14 | Leakage current of PEEK, PTFE, and PI samples with aging time. [Color figure can be viewed at wileyonlinelibrary.com]

Leakage current measurement has been made to access changes in conductivity of PEEK as a result of aging. The leakage current is closely associated with the conductivity of the material. The variation of leakage current density with aging is shown in Figure 14. It can be seen that leakage current density is increased under the action of higher electric field strength. Also, the leakage current density of PEEK has reduced as a result of aging. The relationship of leakage current density (J) and conductivity (σ) under e-field (E) is given as follows:

$$J = \sigma E \tag{5}$$

Also, the conductivity (σ) can be written in terms of charge amount (q), charge carrier mobility (μ), and charge density (n) as follows:

$$\sigma = qn\mu \tag{6}$$

According to the relationships given in Equations (5) and (6), decrease in leakage current density (J) means reduction in conductivity (σ) of material. The lower values of leakage current density (J) observed in the aged samples of PEEK specify that the charge transport is hindered by the degradation that may result in crosslinking network inside the PEEK which is conductive to increase the hardness, brittleness, and carbonization of polymer. This structure will limit the charge carrier mobility and resultant conductivity and leakage current density of PEEK is reduced. The crosslinked structure is not conductive to dielectric polarization and conductivity of PEEK [17, 48].

The variation of AC breakdown strength of PEEK due to aging is shown in Figure 12d. The breakdown strength of PEEK exhibits a progressive increase with aging duration with maximum recorded for samples aged for 170 h (1.6% increase). This phenomenon can be attributed to the structural modifications induced by thermal oxidative aging in PEEK, primarily involving crosslinking. As the aging process progresses, crosslinking in PEEK occurs, leading to a reduction in the mobility of charge carriers within the polymer matrix. This restricted electronic movement results in an increased dielectric strength, as a higher voltage is required to initiate electrical breakdown. Furthermore, the literature also suggests that aging also causes gradual solidification and carbonization of the polymer, which enhances its electrical insulating properties [17]. This could also be the reason for increased breakdown strength as the structural rigidity of PEEK is increased with aging (as observed in DMA analysis), which consequently suppresses the conductive pathways inside PEEK.

3.2 | PTFE

3.2.1 | FTIR Analysis

The change in chemical morphology of PTFE as a result of aging (0–170 h) is recorded in the form of characteristics FTIR spectra and shown in Figure 15. Peak at 1200 cm^{-1} corresponds to the —CF_2— anti-symmetric expansion vibration. Peak at 1146 cm^{-1} is referred to the symmetric expansion and contraction vibration of —CF_2—. The band observed at 1793 cm^{-1} corresponds to the presence of (—CF═CF_2) double bond end groups [54]. The characteristic peaks captured at 718, 738, and 778 cm^{-1} are due to wagging and rocking modes of CF_2 groups present in the amorphous regions of PTFE [55, 56]. The change in the intensity of these bands is correlated with the changes in crystallinity of the PTFE. It can be seen that bands intensity of these bands decrease with aging time. These changes are indicative of a possible decrease in the amorphous part, which can be related to increase in crystallinity of PTFE during aging process. It can be seen from Figure 15 that the peak intensities at 1200 cm^{-1}

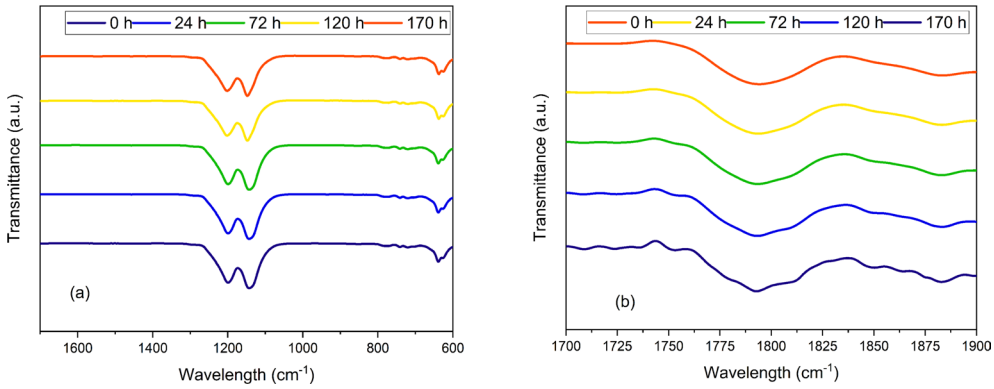

FIGURE 15 | FTIR spectra of PTFE samples with aging time. [Color figure can be viewed at wileyonlinelibrary.com]

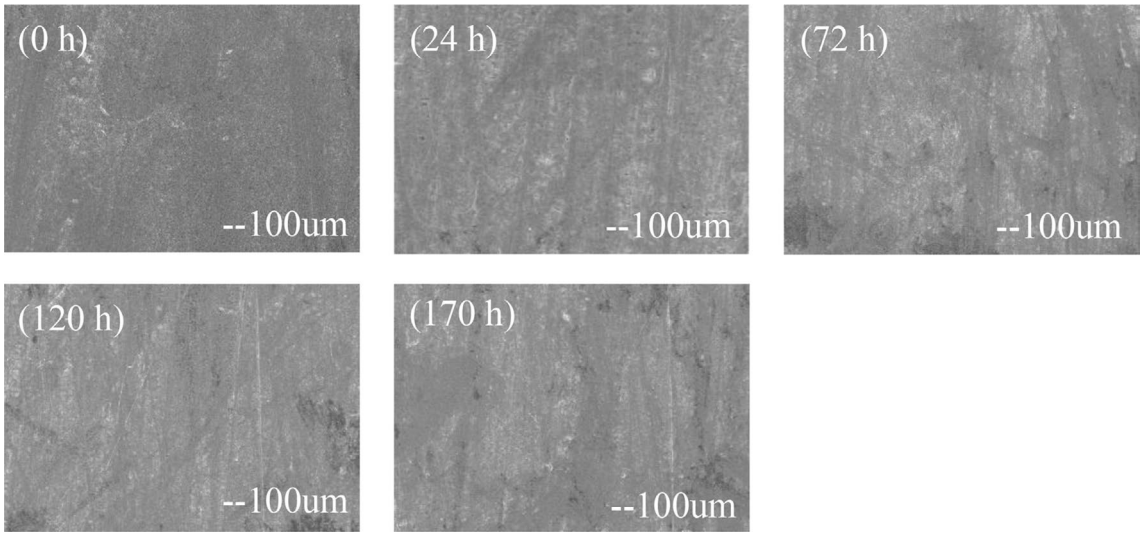

FIGURE 16 | Surface SEM of PTFE samples with aging time.

and 1146 cm^{-1} is decreased with increasing aging time which is indicative of the reduction in the number of —CF_2 groups during aging; meanwhile, a peak at 1793 cm^{-1} appeared as a result of —CF═CF_2 functional groups, as shown in Figure 15b. The results illustrate that these terminal functional groups are already present in unaged PTFE sample, which could be formed during the production process of PTFE material. However, an increase in peak intensities is observed with increase in thermal oxidative aging time. The increase in (—CF═CF_2) terminal double bond groups is attributed mainly to products of chain scissions (breakage of the C—C and C—F bonds) and oxidation reactions by oxygen present in air during the thermal oxidative aging, which leads to the formation of double bonds by bond retraction [18, 54]. The occurrence of chain scission can cause a decrease in the molecular weight, reduction in density, and an increase of the free volume of PTFE polymer [18, 57]. It is worthy to say that no moisture ingression is seen in chemical composition due to hydrophobicity of PTFE and the aging in PTFE is mainly dominated by thermal oxidative stress.

3.2.2 | Microscopic Morphology

Thermal degradation refers to the breaking of molecular chains in engineering plastics when subjected to elevated temperatures over extended periods. The stability of a molecular chain is directly influenced by the bond energy of its constituent chemical bonds, with higher bond energies conferring greater resistance to degradation.

For instance, PTFE, which contains small fluorine atoms, exhibits high C—F bond energy, leading to its exceptional chemical stability. Additionally, thermal degradation is affected by the purity of the polymer; materials with structural instability or impurities are more prone to degradation. To study the effect on aging on microscopic morphology of PTFE, SEM micrographs are taken at same magnifications. It can be seen from Figure 16 that microscopic morphology changes as a result of aging. The surface morphology shows deterioration and degradation voids can be seen. A loose structure with a hole type morphology indicate that the increase in free volume of polymer is observed. As discussed earlier in FTIR, the degradation of polymer chain in form of chain scission can reduce the polymer density and result in an increase in free volume of PTFE which is also highlighted in microscopic morphology of PTFE. Although PTFE aging temperature in this research is below the melting point of PTFE, however, prolonged exposure to high temperatures, combined with the presence of oxygen and humid conditions, can induce surface morphological changes in PTFE. These changes alter its surface properties, likely resulting from the degradation

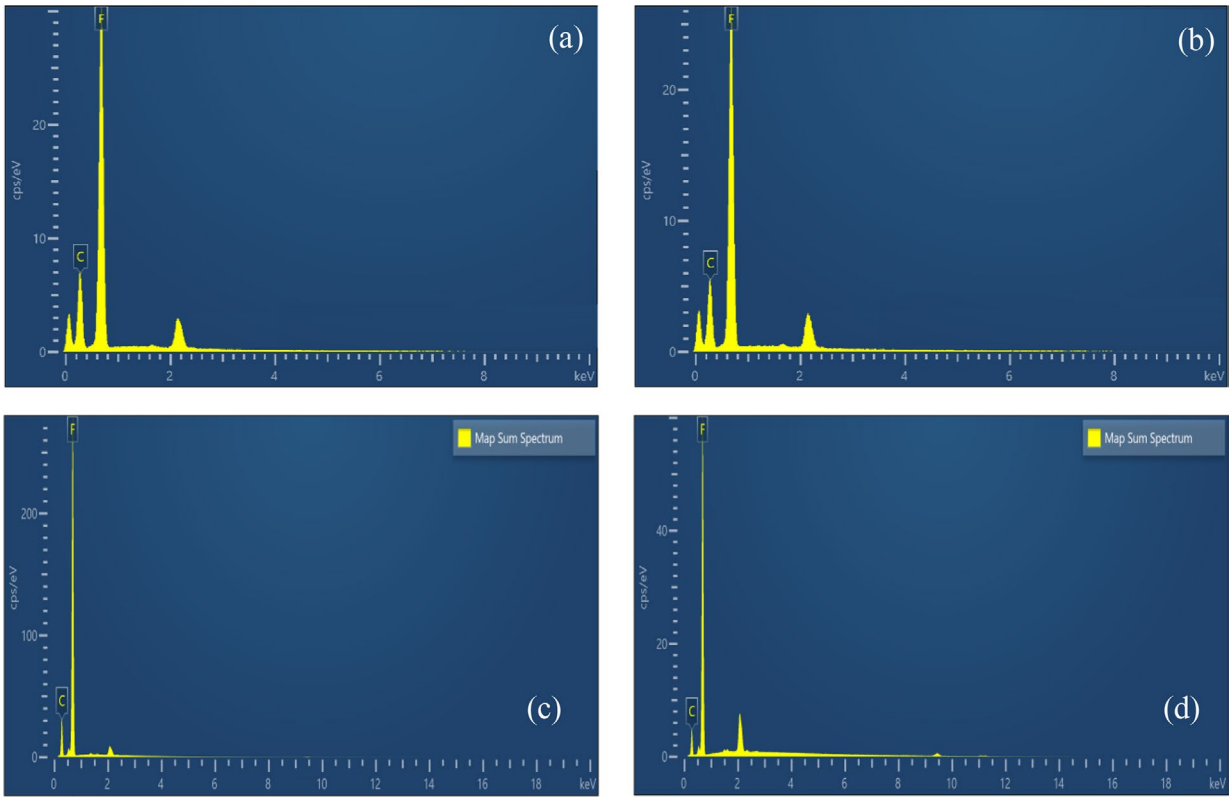

FIGURE 17 | EDS elemental scan of PTFE samples: (a) fresh (surface), (b) aged 170 h (surface), (c) fresh (cross-section), and (d) aged 170 h (cross-section). [Color figure can be viewed at wileyonlinelibrary.com]

TABLE 4A | EDS surface scan data of PTFE samples.

	EDS elemental weight (%)		Weight (%) sigma	
Elements	**PTFE (0 h)**	**PTFE (170 h)**	**PTFE (0 h)**	**PTFE (170 h)**
C	28.09	26.43	0.27	0.41
F	71.91	73.57	0.27	0.41

of molecular chains during thermal oxidative aging. The loss of small molecules weakens the interactions between polymer chains, leading to a looser structure. The elemental weight percentages also change as a result of aging which is highlighted in Figure 17. It can be seen from EDS data listed in Table 4a that the fluorine content is increased and the carbon elemental content is reduced as a result of aging. The changes in the EDS elemental content values are also indicative of degradation of main chain of PTFE (breakage of C—C bond) as discussed in FTIR results. The increase in fluorine content detected by EDS on surface may act as shield layer and prevent PTFE from further oxidization in matrix [57].

The cross-sectional SEM micrographs of PTFE samples are shown in Figure 18. Results show obvious structural changes, as highlighted from SEM and image analysis. These changes can be attributed to chain scission and surface oxidative degradation. The fresh PTFE sample in Figure 18a displayed a smooth and homogeneous surface with minimal defects. In contrast, the aged sample in Figure 18c exhibited a rough and uneven texture, with prominent cracks and fissures. The PTFE-aged sample seems more fragmented and less cohesive compared to the fresh PTFE sample. Sobel edge detection in Figure 18e reveals structural damage with irregularities and disrupted regions, showing a greater density of cracks and structural inconsistencies. The SEM results in Figure 18d indicate the formation of voids and microstructural gaps. These voids result from the loss of molecular weight due to chain scission. The increased free volume also reflects the reduced packing efficiency of the polymer, which compromises its mechanical properties. The EDS mapping results in Figure 17 reveal a reduction in carbon content and a relative increase in fluorine content in the aged PTFE samples. The cross-sectional SEM EDS results in Table 4b are consistent with surface SEM EDS results. Carbon to fluorine (C:F) ratio is reduced due to aging. This chemical shift suggests that thermal aging caused selective degradation of the carbon backbone, likely due to cleavage of C—C bonds. This degradation process is consistent with oxidative degradation pathways observed in PTFE.

The morphological and chemical changes observed in the aged samples are indicative of thermal oxidative degradation. The increased porosity and roughness are direct consequences of these processes, reducing the material's overall stability and performance.

The optical morphology of aged PTFE from POM in Figure 17 also shows pinholes and a loose structure representation due to aging. As aging progresses, visible microcracks and voids can also be seen in Figure 19, which suggest mechanical degradation. These changes are possibly caused by thermal stress and oxidation. The optical photos also show slight change in color

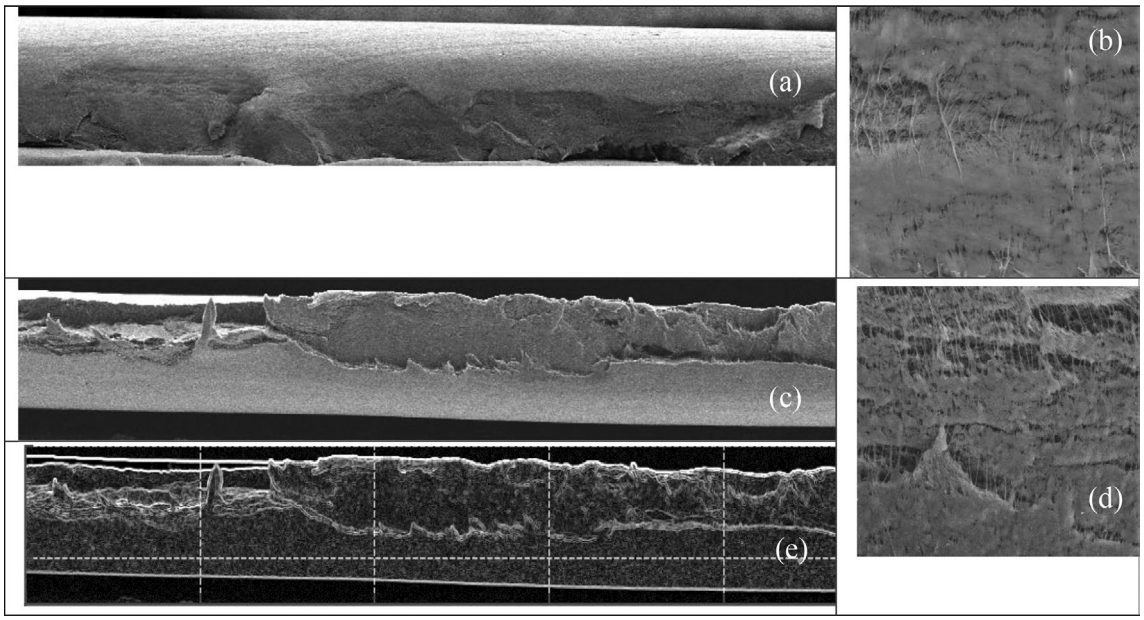

FIGURE 18 | Cross-sectional SEM of PTFE samples: (a and b) PTFE 0 h, (c and d) PTFE 170 h, and (e) Sobel edge detection PTFE 170 h.

TABLE 4B | EDS cross-section scan data of PTFE samples.

	EDS elemental weight (%)		Weight (%) sigma	
Elements/ ratio	**PTFE (0 h)**	**PTFE (170 h)**	**PTFE (0 h)**	**PTFE (170 h)**
C	32.25	27.34	0.11	0.26
F	67.75	72.66	0.11	0.26
C:F ratio (atomic)	0.75	0.60		

of PTFE which could be a sign of surface oxidation but visual inspection shows no obvious color change.

3.2.3 | Mechanical Properties

Aging under thermal oxidative conditions can affect the mechanical properties of insulation materials. To study the change in mechanical properties of PTFE as a result of aging, tensile strength and elongation (%) is recorded and shown in Figure 20a. Stress and strain curve of PTFE samples are presented in Figure 20b. It can be seen from Figure 20a that tensile strength of PTFE shows a decline with progress of aging. The tensile strength of PTFE finally reduced to 26 MPa at the end of aging period. The change in breaking elongation of PTFE due to aging is highlighted in Figure 20a. A slight increase in the breaking elongation observed at the beginning of aging period (0–72 h) can be correlated to the damage degree of PTFE molecular chains which is particularly low in the beginning of aging period. With the progress of aging period, the breaking elongation tends to decrease after 72 h which can be associated to the enhancement in the damage degree of PTFE molecular chains [58]. After 170 h, the breaking elongation of PTFE reaches to the value of 293%. As a part of conclusion, it can be said that the reduction in mechanical properties of PTFE as a result of aging was attributed to the destruction of molecular chain mainly in form of breaking (scission). This phenomenon also weakens the intermolecular forces and result in reduction of molecular weight of PTFE, decreasing its mechanical properties.

DMA results (storage modulus and loss tangent) for PTFE samples are shown in Figure 20c,d. The high values of storage modulus are observed in the PTFE at lower temperatures (< 100°C) which are attributed to the restricted motion of polymer chain segments, as most of the polymer remains frozen at low temperature due to the tight packing of atoms. This enables the material to store more energy, resulting in elevated modulus values [59]. However, modulus decreases with increasing temperature across all regions, which is attributed to the enhanced mobility of components, leading to a loss of their closely packed configuration and a significant reduction in storage modulus near the glass transition temperature of PTFE (α transition temperature, which is related to molecular mobility of the amorphous phase of PTFE) [60]. It can be seen from DMA results in Figure 20c that the storage modulus decreases as the aging time increases (from 0 to 170 h), particularly at higher temperatures. Thermal oxidative aging causes chain scission in PTFE resulting in small fragments, reducing the overall molecular weight. This leads to fewer entanglements and reduced stiffness, which lowers the storage modulus.

Tan δ curves of PTFE samples are shown in Figure 20d. It can be seen from the results that the height of the tan δ peak increases with aging time and the peak position slightly shifts to lower temperatures (from 127.4°C to 126.5°C) with aging (0–170 h). Thermal oxidative aging results in chain scission in PTFE creating shorter chains and voids which facilitates segmental motion of polymer chains. The amorphous regions of polymer experience less restriction and molecular mobility is enhanced consequently. Shorter chains also require less thermal energy to achieve

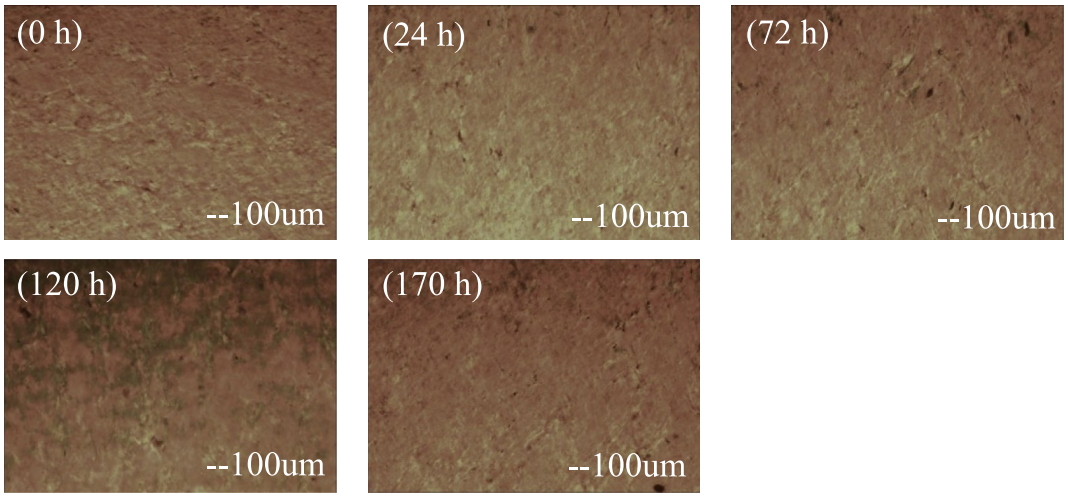

FIGURE 19 | POM of PTFE samples with aging time. [Color figure can be viewed at wileyonlinelibrary.com]

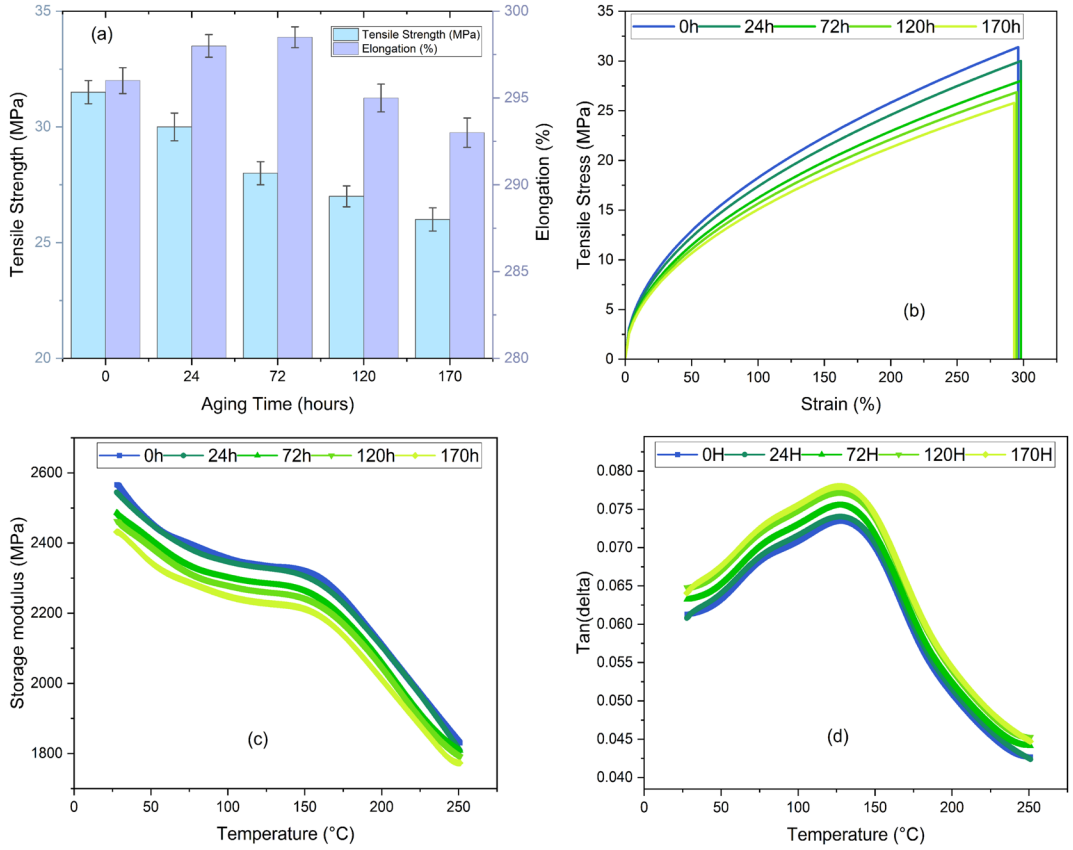

FIGURE 20 | Mechanical properties of PTFE samples with aging time: (a) tensile and elongation, (b) stress versus strain curves, (c) DMA storage modulus, and (d) DMA tan δ. [Color figure can be viewed at wileyonlinelibrary.com]

mobility, leading to a decrease in the temperature required for segmental motion (i.e., decrease in T_g). Reduced stiffness and modulus suggest that the PTFE high-load bearing capability is compromised after aging (PTFE becomes less rigid).

3.2.4 | DSC and TGA Analysis

The TGA and DTG curves of PTFE unaged and aged samples have been shown in Figure 20. In PTFE, the bond energy of C—F bonds (507 kJ/mol) is higher than that of C—C bonds which is 348 kJ/mol, meaning the weaker C—C bonds will break first when exposed to high temperatures. The mechanism for PTFE pyrolysis most likely involves end-chain scission of C—C bonds, producing radicals and forming TFE monomers through an "unzipping reaction" [61]. As a result, small molecules usually evaporate into the gas phase during heating process, which leads to a reduction in sample weight. It can be seen from TGA curves in Figure 20a that PTFE appears stable with no weight loss observed until 488°C. After this temperature, the thermal

degradation of PTFE starts and a weight loss of 5% ($T_{5\%}$) is observed in PTFE around 532°C. There is no significant change in weight loss (%) of PTFE as a result of aging. PTFE finally loses all its weight around 620°C which is almost same for aged PTFE. Similarly, the maximum decomposition of PTFE shows no significant difference during aging as highlighted in Table 5.

In order to study the change in melting and crystallization behavior of PTFE as a result of aging, DSC melting curves are measured and shown in Figure 21c. The DSC data is listed in Table 6. It can be seen that there is a slight increase in the peak melting temperature (T_p) of PTFE as a result of aging. It can be observed from the results that the melting temperature and shape of the DSC melting curve of PTFE are not significantly influenced by aging. The area under the endothermic melting peak (melting enthalpy ΔH_m), which is related to the degree of crystallinity, is higher in aged PTFE when compared with unaged PTFE samples. The degree of crystallinity PTFE as a result of aging is increased. This phenomenon can be attributed to the formation of smaller molecules which resulted from end-chain scission of macromolecules during aging. This process may lead to a reduction in molecular weight, and can increase chain mobility and/or promote crystallization process within the polymer amorphous regions. The behavior of PTFE observed in DSC experiments is consistent with the results discussed in FTIR.

3.2.5 | Optical UV–Vis Spectrum Analysis

UV–vis can be used to access the change in optical characteristics of polymers due to aging. As mentioned previously, it highlights the changes in the electronic excitation states between the energy levels of a material which can be correlated to the electrical properties of a material. The UV–vis spectra of PTFE samples is shown in Figure 22. The spectra of PTFE shows no red or blue shift as a result of aging. However, increase in absorption is recorded especially in the UV region in aged samples.

TABLE 5 | TGA and DTG data of PTFE samples.

Aging time (h)	$T_{5\%}$ (°C)	T_{max}	R_w
0	532.0	588.6	0
170	531.7	589.0	0

Chain scission reduces the molecular weight of PTFE, resulting in smaller polymer fragments or monomers. These smaller fragments may have the capability to absorb more light especially in the UV region (typically in 200–300 nm). In addition, as discussed in SEM results, aging can lead to the formation of pinholes, voids, and imperfections in PTFE. This would cause increased scattering of light in the visible region, leading to increase in absorbance across the entire spectrum, especially in the visible region (400–800 nm).

It has been reported in literature that the occurrence of various phenomena such as chain scission, structural disorder, and formation of free radicals can decrease the optical band gap of polymer [57]. To study the change in optical band gap as a result of PTFE aging, optical band gaps of PTFE samples (unaged and aged) were calculated using Equation (4) and highlighted in Figure 22b. It can be seen that the band gap of PTFE has reduced from 5 to 4.8 eV as a result of aging. The increase in absorbance and reduction of optical band gap of PTFE indicate that localized electronic states were induced between energy levels of PTFE. The presence of such localized states acts as hopping sites of electronic carriers which may promote motion of charge carriers along polymer chains. In order words, the electrical conductivity of PTFE can be affected as a result of aging.

3.2.6 | Dielectric Analysis

PTFE is considered as nonpolar or apolar dielectric materials. The main contribution to the relative permittivity of PTFE is usually considered to be the electronic polarization [62]. As said earlier, the C—F bond in PTFE exhibits exceptional stability but

TABLE 6 | DSC data of PTFE samples.

Aging time (h)	T_p (°C)	ΔH_m (J/g)	X_c (%)
0	326.2	35.1	42.8
24	327.0	36.3	44.2
72	327.3	36.0	44.0
120	328.0	37.5	45.7
170	328.4	39.0	47.5

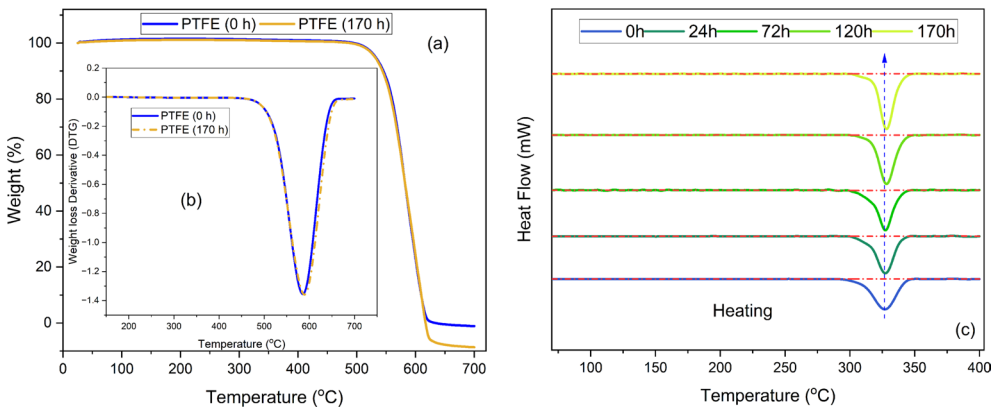

FIGURE 21 | Thermal analysis curves of PTFE samples: (a) TGA, (b) DTG, and (c) DSC. [Color figure can be viewed at wileyonlinelibrary.com]

due to high electronegativity of fluorine in PTFE, the intermolecular forces of PTFE become relatively low. This allows the PTFE to expand when heated owing to its high coefficient of linear expansion.

BDS results of PTFE are drawn in Figure 23a,b. The results show that the dielectric constant of PTFE decreases consistently

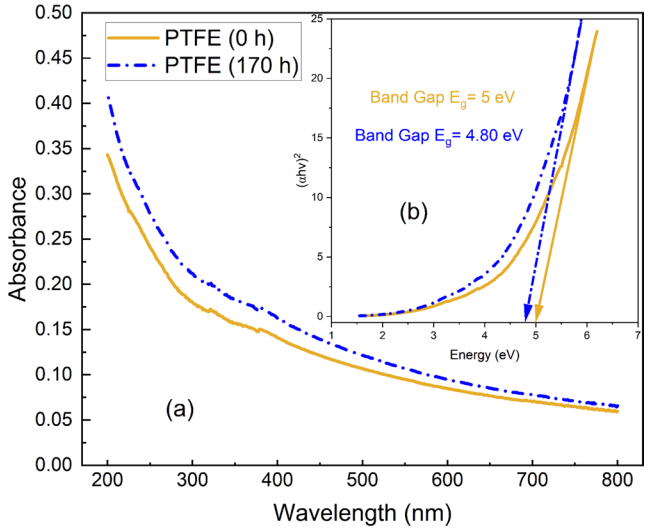

FIGURE 22 | UV–vis spectra of PTFE samples: (a) spectra; (b) Tauc plot. [Color figure can be viewed at wileyonlinelibrary.com]

with aging time, reflecting structural degradation such as chain scission in PTFE. Chain scission reduces molecular weight and introduces free volume, lowering the overall polarizability of the material. This phenomenon is evident in the steady reduction in the dielectric constant of PTFE from 0 to 170 h of aging. The tan δ (dielectric loss) results in Figure 23b reveal further insights into the molecular dynamics of aged PTFE. The increase in tan δ with aging indicates enhanced molecular mobility and energy dissipation, particularly at lower frequencies. Aging has facilitated localized motions in PTFE which promoted the relaxation process in PTFE due to increased localized mobility as discussed in DMA analysis. Conductivity loss in PTFE is increased which is more prominent at the later stage of aging (120–170 h) which may be due to electronic conduction dominated by electronic carriers (electrons and holes). The variation of the relative permittivity of PTFE with progress of aging is shown in Figure 23c with a temperature sweep (20°C–200°C). The relative permittivity of all samples decreases with increase in temperature. Also, the relative permittivity of PTFE recorded at room temperature decreases from 2.1 to 1.9 with the progress of aging (0–170 h), and a similar trend is observed at high temperature, for example, 200°C. This clarifies that the electronic polarization ability of PTFE reduces due to aging as evident from polarization charge density plots in Figure 24. As mentioned earlier, the chain scission in PTFE due to aging can cause the decrease in density and molecular weight of polymer. Thermal expansion of PTFE also occurs in PTFE which results in less number of molecules per unit volume [19]. Due to aging, the free volume of PTFE also

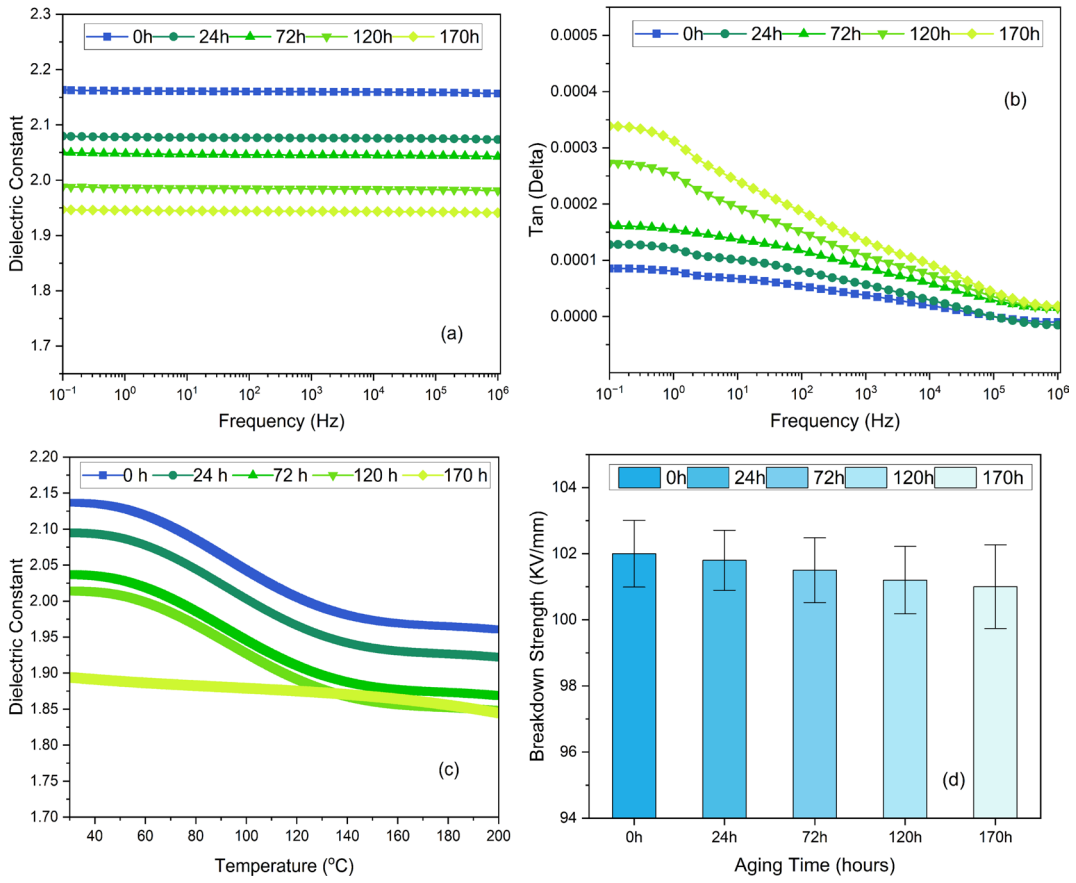

FIGURE 23 | Dielectric properties of PTFE samples with aging time: (a) dielectric constant, (b) dielectric loss, (c) dielectric constant versus temperature, and (d) AC breakdown strength. [Color figure can be viewed at wileyonlinelibrary.com]

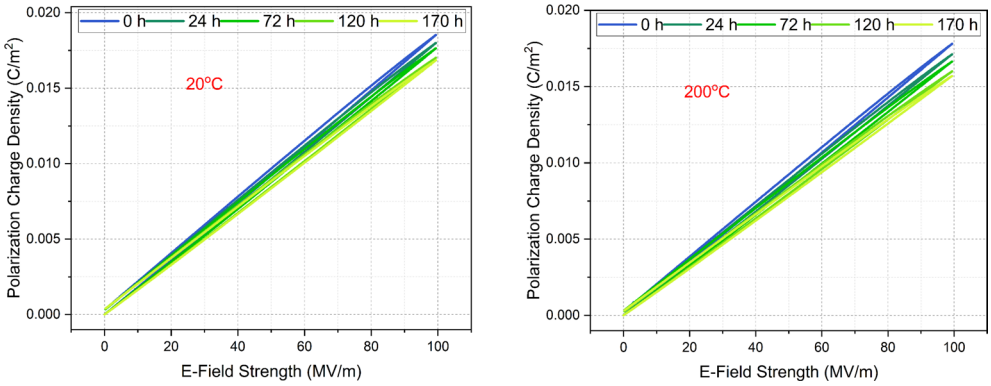

FIGURE 24 | Polarization of PTFE samples with aging time at room temperature and 200°C. [Color figure can be viewed at wileyonlinelibrary.com]

increases which results in less number of molecules in a unit volume responsible for polarization in PTFE. As a result, the polarization charge density and relative permittivity of PTFE decreases.

Leakage current density measurements of PTFE unaged and aged samples have been done and the result are drawn in Figure 14. It can be seen from results that there is no significant difference in the leakage current density of PTFE in the beginning of aging. As mentioned before, the apolar nature of PTFE makes it susceptible only to electronic polarization which is not conductive to energy dissipation in PTFE. Since the conductivity of PTFE is very low, therefore no significant differences can be seen at early stage of aging. At a later stage of aging, the leakage current increases in PTFE and similar trend is recorded for 50 and 100 MV/m field strengths. The increase in the leakage current density can be related to increase in the conductivity of PTFE by the relationship mentioned in Equations (5) and (6). In general, the electrical conduction property in polymers like PTFE is dominated by electronic carriers (electrons and holes) at low temperatures. These electronic carriers usually impart a strong positive dependence on electric field intensity [50]. The increase in the conductivity of PTFE at a later stage of aging can be correlated to the plentiful generation of electronic localized states as mentioned earlier in UV–vis analysis. These localized states can act as hopping sites for electronic carriers and can promote charge carrier motion and transition along PTFE polymer chains from one molecule to other via electronic hopping process [57]. Thus, aging increases charge mobility in PTFE which increases the conductivity and leakage current of PTFE.

The effect of thermal oxidative aging on the AC breakdown strength of PTFE is shown in Figure 23d. It can be seen that the thermal oxidative aging has a slight impact on the AC breakdown strength of PTFE as evidenced by a slight decline in dielectric performance over increasing aging duration. The breakdown strength of PTFE reduces from 102 to 101.1 kV over the aging period (0–170 h). The observed reduction in breakdown strength is primarily attributed to the degradation of the PTFE polymer matrix through chain scission, which disrupts the molecular structure and weakens the dielectric integrity of PTFE. As thermal exposure progresses, PTFE undergoes volume expansion, leading to a decrease in molecular density. This reduction in the number of molecules per unit volume results in an increased mean free path for charge carriers, thereby facilitating electron impact ionization. Consequently, the likelihood of electrical breakdown is enhanced in PTFE, as the material becomes more susceptible to localized dielectric failure. The experimental trend aligns with existing literature, which suggests that aging leads to structural deterioration, making the PTFE more prone to electrical degradation [19].

3.3 | PI

3.3.1 | FTIR Analysis

In order to study change in the chemical morphology of PI, FTIR spectra of PI samples is recorded. The change in FTIR spectra of PI during aging is highlighted in Figure 25. The FTIR spectra shows several characteristic peaks that corresponds to imide functional groups (C—N at 1372 cm^{-1}, and C═O at 721 cm^{-1}) in PI. The peaks around 825 and 885 cm^{-1} bands are associated with hydrogen out-of-plane vibrations of the aromatic rings. These peaks show an obvious decreasing trend during aging which means that the aromatic rings of PI can be subjected to possible oxidation and imide ring structure can encounter degradation due to aging. In addition, the broad characteristic peak of ether functional group (C—O—C at 1100–1000 cm^{-1}) also shows a decreasing tendency with aging progress. In comparison, the stretching vibration peaks of C═C bond in the benzene ring observed at 1496 cm^{-1} and functional group (—CONCO at 1711 cm^{-1}) keep relatively stable, which indicates that these two functional groups exhibit comparatively higher stability during the thermal aging. Increase in band transmittance around 3500 cm^{-1} as highlighted in Figure 25b suggests the formation of OH groups which is indication of moisture ingression in PI [63].

The relative changes of the 1230 and 3500 cm^{-1} bands are indicative of the possible cleavage of the aryl ether bonds and deterioration of imide ring structure in PI. Overall, the FTIR results highlight scission of ether bonds with possible breaking and oxidization of some of C—H bonds in aromatic rings while the imide ring structure in PI can be subjected to degradation. It is worthy to say that the aging in PI is imparted both by thermal oxidative stress and humidity.

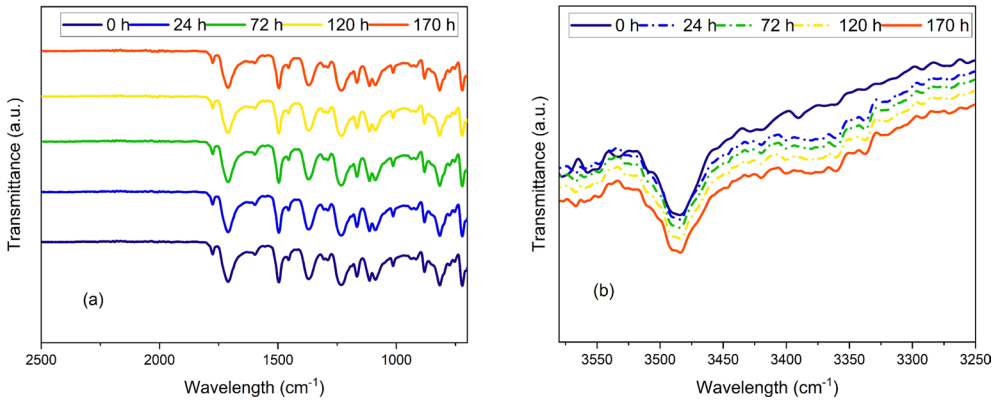

FIGURE 25 | FTIR of PI samples with aging time. [Color figure can be viewed at wileyonlinelibrary.com]

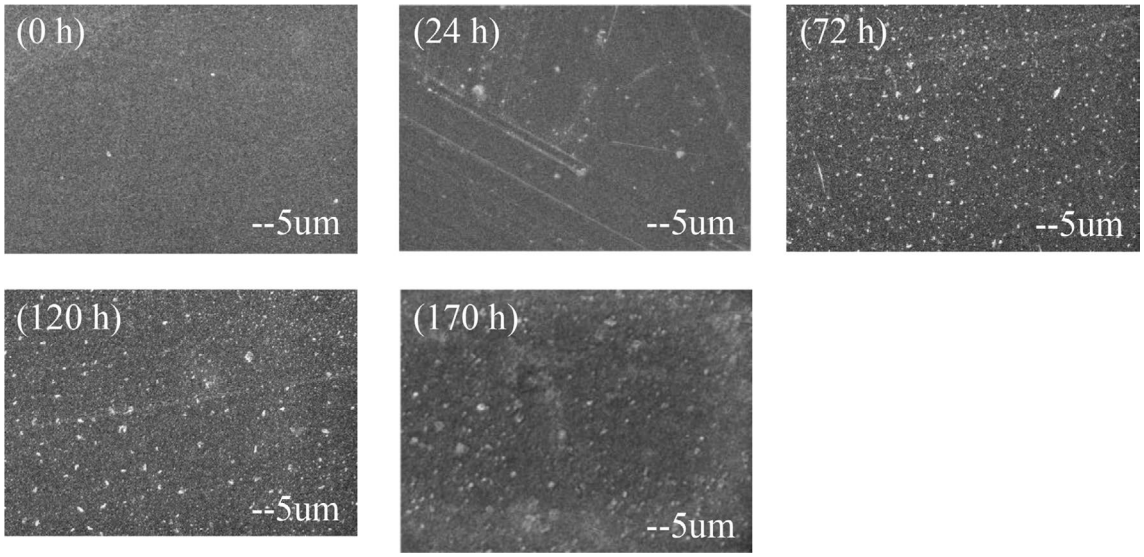

FIGURE 26 | SEM of PI samples with aging time.

3.3.2 | Microscopic Morphology

The change in surface morphology of PI as a result of aging is highlighted in Figure 26. It can be seen from Figure 26 that the surface morphology of PI unaged appears smooth with no noticeable imperfections. In contrast, the surface morphology of aged PI shown in Figure 26 shows microvoids, pits, and imperfections. A granular type morphology can be seen in SEM of PI-aged samples. Some tiny crack paths with a size of few microns also appear in PI samples with aging progress indicating thermal stress-induced damage. These microcracks can propagate with further aging and promote moisture ingress in bulk, compromising the material structural and dielectric properties. The EDS surface elemental analysis in Figure 27 shows an increase in oxygen content which can be referred to the surface oxidation of PI during aging, as mentioned previously. In contract, EDS data in Table 7a show a slight reduction in carbon content with decrease in nitrogen content, observed due to aging.

SEM cross-sectional micrographs of PI samples are shown in Figure 28. The aged sample of PI in Figure 28c shows significant degradation (marked in red), with clear evidence of surface roughening, microcracks, and peeling. This suggests oxidation-induced material embrittlement. These voids act as stress concentration points, accelerating crack propagation, and mechanical deterioration. The aged sample of PI shows material fragmentation and increased roughness as evident in Figure 28e, consistent with oxidative degradation. The observed surface peeling suggests a breakdown of the polymer backbone and formation of low-mass polar molecules in PI during thermal aging. The marked region in the aged PI bulk shown in Figure 28d are likely oxidation by-products, impurities, or moisture-induced residues from degradation processes. The elemental analysis via EDS shown in Figure 27 provides insight into the chemical changes induced by thermal oxidative aging in PI. The EDS cross-section data in Table 7b show that carbon content has decreased from 72.27% to 71.60%, suggesting oxidation-induced degradation of PI polymer backbone. The decline in C:N atomic ratio (from 13.10 to 11.60) further supports the degradation of aromatic rings in diphenyl ether structures, which typically occurs during oxidative aging. The decrease in C:N atomic ratio aligns with literature reports that aromatic ring degradation in diphenyl ether units contributes to this reduction [64]. The C:O atomic ratio decreased from 4.52 to 4.47, further supporting the idea that oxidative degradation of the polymer backbone took place during aging. Overall, SEM observations are indicative of noticeable degradation of PI polymer bulk (chain scission) and oxidation-induced embrittlement. These

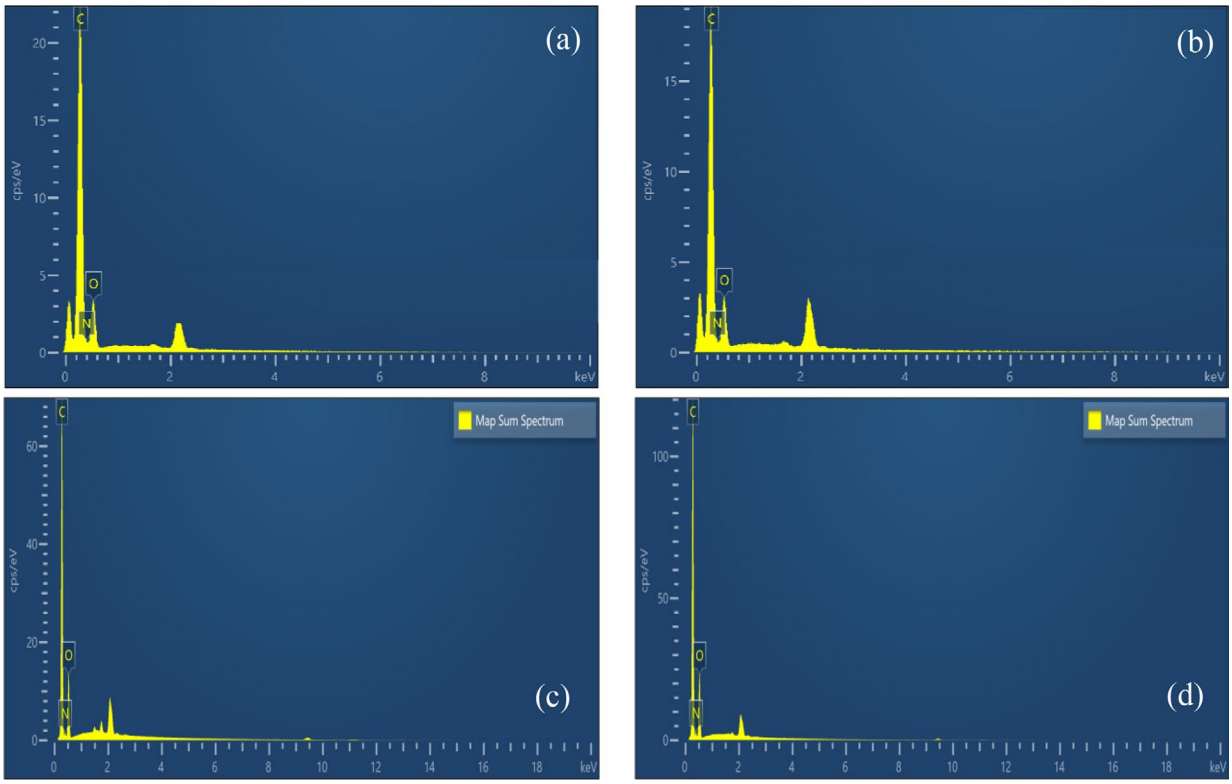

FIGURE 27 | EDS elemental scan of PI samples: (a) fresh (surface), (b) aged 170 h (surface), (c) fresh (cross-section), and (d) aged 170 h (cross-section). [Color figure can be viewed at wileyonlinelibrary.com]

TABLE 7A | EDS surface scan data of PI samples.

	EDS elemental weight (%)		Weight (%) sigma	
Elements	**PI (0 h)**	**PI (170 h)**	**PI (0 h)**	**PI (170 h)**
C	71.29	71.03	1.75	1.88
O	22.75	23.45	0.60	0.65
N	5.97	5.49	0.21	0.24

chemical and structural changes may deteriorate mechanical performance of PI.

The optical photos in Figure 29 show surface of aged PI shows developed dark spots and voids both in horizontal and vertical directions in aged samples. The surface of samples in Figure 29 appears mostly uniform with minor imperfections, suggesting that aging has not caused extensive surface roughness. However, small scattered defects or impurities are visible in aged samples, which may be early signs of degradation. The POM and visual inspection also highlighted the change in color of PI films. It can be seen from results that the color of original PI sample has changed from light brown to brown and the transparency is reduced also. The slight change in color and the reduction in the transparency of PI observed as a result of aging can be referred to the formation of microvoids and oxidation of aromatic rings (as said in FTIR). Similar results were observed about the morphology analysis of PI in literature reported previously [65].

3.3.3 | Mechanical Properties

The effect of aging on the mechanical properties (tensile strength and elongation [%]) of PI is shown in Figure 30. A clear decrease of tensile strength with progress of aging can be seen. After 170 h of thermal oxidative aging, PI loses 54% of its tensile strength. The breaking elongation (%) also decreases gradually with aging. The elongation at break (%) finally reduced to 16% after 170 h of thermal oxidative aging. The reduction in mechanical properties of PI can be referred to degradation of imide ring structure and breaking of ether linkage with possible breakage of some of aromatic C—H bonding as discussed earlier in FTIR results. This weakens the intermolecular forces and PI can be subjected to breaking under mechanical stress. The appearance of microcrack paths in SEM results due to aging also validates the reduction in breaking elongation of PI and indicates the occurrence of embrittlement in PI.

3.3.4 | DSC and TGA Analysis

The change in thermal stability and weight loss due to aging is recorded in terms of TGA of PI samples. During thermal decomposition, by-products consists low-mass molecules usually of volatile and nonvolatile nature. The volatile products usually escape with progress of thermal decomposition. The results in Figure 31a show that the weight loss remain stable till 300°C. After this temperature, weight loss tends to increase in PI samples due to enhancement of thermal pyrolysis process in PI. It can be seen from the results that PI samples begin to lose mass quickly around 550°C. The temperature at which 5% weight loss

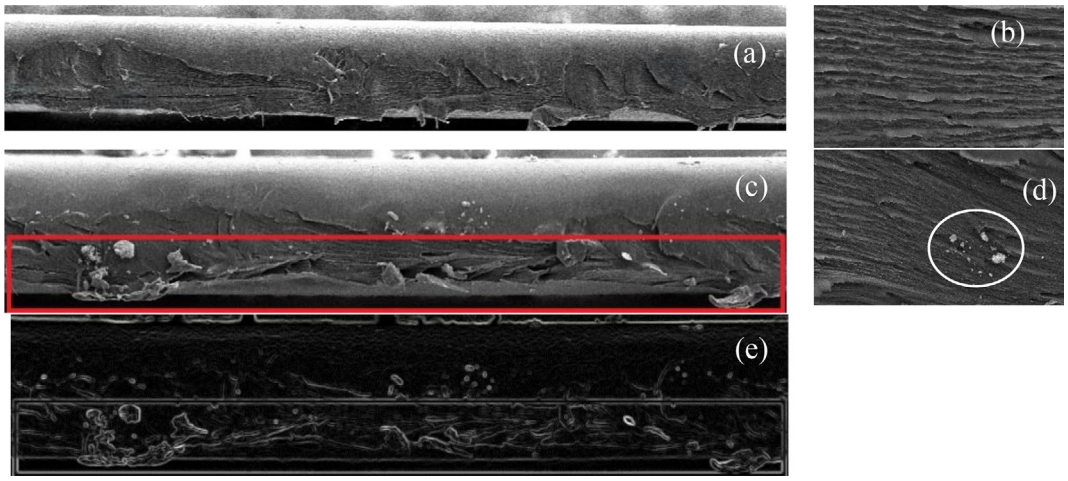

FIGURE 28 | Cross-sectional SEM of PI samples: (a and b) PI 0 h, (c and d) PI 170 h, and (e) Sobel edge detection PI 170 h. [Color figure can be viewed at wileyonlinelibrary.com]

TABLE 7B | EDS cross-sectional scan data of PI samples.

	EDS elemental weight (%)		Weight (%) sigma	
Elements/ratio	**PI (0 h)**	**PI (170 h)**	**PI (0 h)**	**PI (170 h)**
C	72.27	71.60	0.35	0.26
O	21.26	21.31	0.16	0.12
N	6.42	7.15	0.42	0.31
C:O ratio (atomic)	4.52	4.47		
C:N ratio (atomic)	13.10	11.60		

is recorded for unaged PI samples is 584°C (onset temperature). A decrease in onset temperature is observed due to aging of PI which is 580°C as listed in Table 8. This decreasing tendency is due to the escape of some low-mass molecules after thermal decomposition which is mainly due to further enhancement of thermal pyrolysis process at high temperature. The DTG shown in Figure 31b records the temperature at which maximum decomposition occurs for PI samples, and values are also listed in Table 8. It can be observed that PI samples show maximum weight loss between 600°C and 650°C. It is evident from DTG results that there is an increase in the maximum decomposition temperature of PI as a result of aging, though the increment is small (~1.5°C). At high temperature, an intense thermal decomposition take place that results in amorphous carbon structure of PI. The TGA experiment ends around 700°C but still there is a residual yield left in PI samples which is higher in case of aged PI samples (54%). This is usually referred to the formation of polar molecules with benzene ring structure during thermal aging process [65].

The DSC heating curves of PI samples is plotted in Figure 32. The PI samples show a weak representation of glass temperature which is observed around 310°C. The results show no noticeable difference in shape of the DSC curve. The glass transition temperature recorded is almost similar for all PI samples tested. The aging causes no significant impact on glass transition temperature of PI.

3.3.5 | Optical UV–Vis Spectrum Analysis

UV–vis absorption spectrum is recorded in order to study the effect of aging on optical properties of PI. There is no noticeable change in the UV–vis spectra of PI observed as a result of aging as shown in Figure 33a. No red or blue shifts are seen in UV–vis spectra due to aging. For further analysis, the values of optical band gaps are obtained using the relationship given in equation. The optical band gap of PI is obtained by extrapolating the linear part of the plot of $(\alpha h\nu)^{0.5}$ with photon energy as shown in Figure 33b. In case of PI, the optical band comes out to be 2.3 eV which is almost similar to optical band gap of aged samples. It can be said from the results of UV–vis results that there are no remarkable changes in the electronic excitation states between the energy levels of PI. In conclusion, the study of UV–vis of PI due to aging does not throw light on the change in electrical properties of PI as a result of aging.

3.3.6 | Dielectric Analysis

BDS plots of PI samples are shown in Figure 34a,b. It can be observed from the results that the dielectric constant of PI decreases slightly with increasing frequency for all aging durations, attributing to the frequency dependence of polarization mechanisms [66]. Also, aging leads to a gradual increase in the dielectric constant of PI, with the 170 h aged sample showing the highest value. Aging in PI likely results in the formation of low-mass polar molecules (e.g., due to oxidative degradation). These molecules increase the dielectric constant due to enhanced dipole moments.

The tan δ in Figure 34b remains stable at lower frequencies but begins to increase at higher frequencies for all PI samples. A noticeable trend is observed where the loss tangent increases

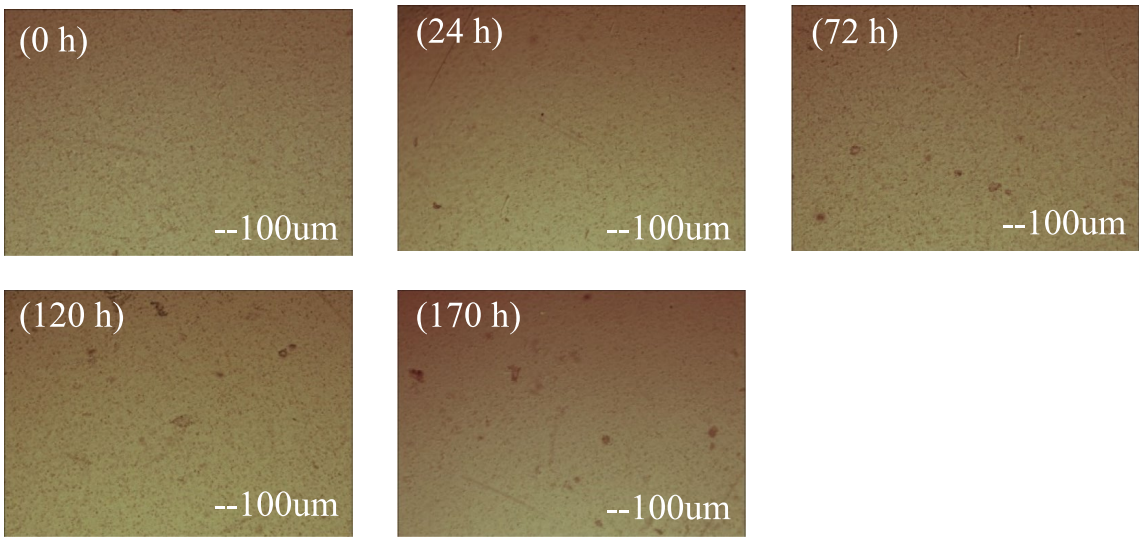

FIGURE 29 | POM of PI samples with aging time. [Color figure can be viewed at wileyonlinelibrary.com]

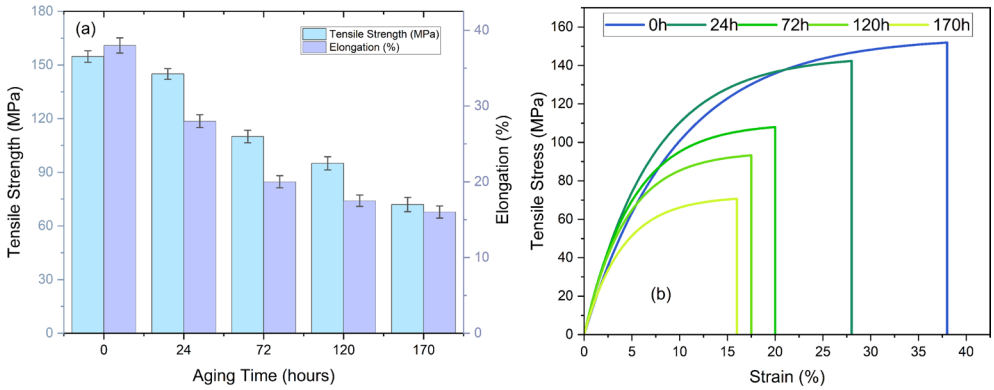

FIGURE 30 | Mechanical properties of PI samples with aging time: (a) tensile and elongation and (b) stress versus strain curves. [Color figure can be viewed at wileyonlinelibrary.com]

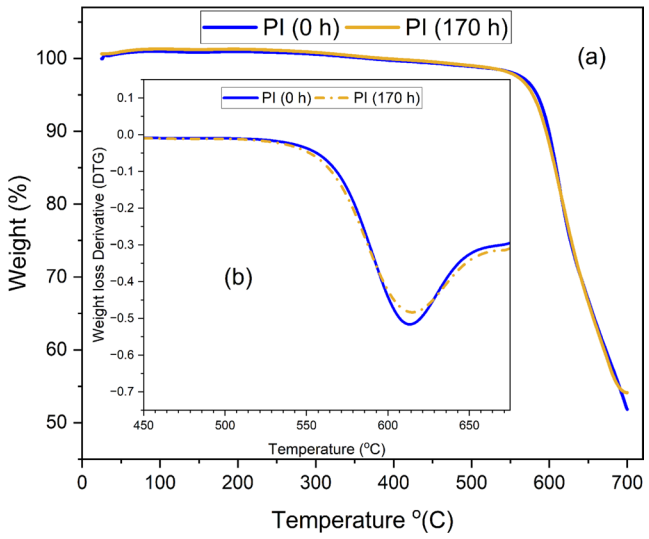

FIGURE 31 | Thermal decomposition curves of PI samples: (a) TGA and (b) DTG. [Color figure can be viewed at wileyonlinelibrary.com]

with aging, particularly for the 120 h and 170 h samples. The polar units produced as a result of aging in PI requires a time

TABLE 8 | TGA and DTG data of PI samples.

Aging time (h)	$T_{5\%}$ (°C)	T_{max}	R_w
0	584.0	613.5	51.4
170	580.0	615.0	54.0

for orientation or displacement. These polar molecules could not keep up with the variation of applied electric field and results in increase in dissipation factor. Due to aging, moisture absorption in PI also increases, introducing additional polar groups (e.g., —OH from moisture) as discussed in FTIR analysis. These groups contribute to both the dielectric constant and loss tangent, particularly at high frequencies where dipolar relaxation mechanisms dominate in PI. The change in dielectric permittivity of PI samples with progress of aging in temperature windows (20°C–200°C) is shown in Figure 34c. It has been reported that the dipolar orientation polarization is a dominant mechanism that accounts for relative permittivity of PI [67]. It can be seen from results that relative permittivity of PI samples decrease with increase in temperature. The measurement results also show that the relative permittivity of PI recorded at room

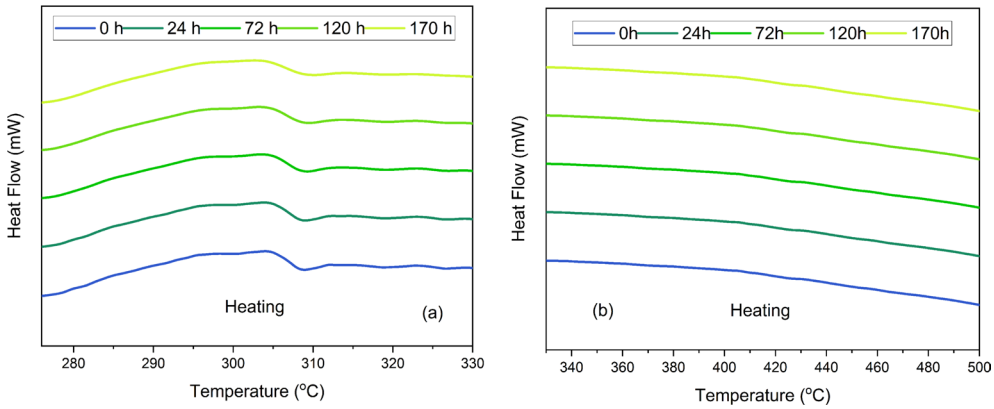

FIGURE 32 | DSC heating curves of PI samples. [Color figure can be viewed at wileyonlinelibrary.com]

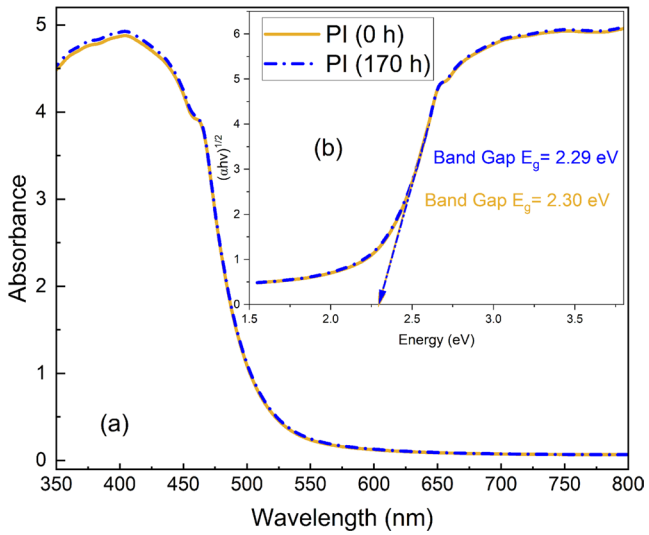

FIGURE 33 | UV–vis of PI samples: (a) spectra; (b) Tauc plot. [Color figure can be viewed at wileyonlinelibrary.com]

temperature increases from 3.2 to 3.7 with increase in aging time (0–170 h). At high temperature of 200°C, similar increase of relative permittivity (from 2.8 to 3.2) is recorded.

To study the change in relative permittivity due to aging, polarization charge density is also recorded for PI samples in Figure 35. The relative permittivity at a certain frequency, for example, 50 Hz is dependent on degree of polarization which is influenced by many factors, for example, free volume, presence of polar groups, etc. It can be seen from polarization results that the degree of polarization of PI due to aging is increased. The polarization charge density results reflect that the polar components responsible for polarization in polymer material has increased. This has increased the charge density and polarizability of PI under the influence of electric field. Aging results in the formation of low-mass polar molecules with free radicals in PI. These mainly include aromatic nitriles, aniline, toluidine, and polar OH groups (due to moisture absorption). These polar molecules increase the degree of polarization and eventually increasing the dielectric permittivity of PI [68].

It is well known that insulating properties, for example, electric conductivity of PI is affected by the change in its dielectric constant [69]. The influence of aging on the leakage current density of PI samples is shown in Figure 14. The results clearly show the increase of leakage current density of PI with aging progress (0–170 h). In addition, thermal aging affects the leakage current more under the influence of high electric field, for example, at 100 MV/m, resulting in higher value of leakage current when compared to the leakage current recorded at 50 MV/m. The thermal aging process results in the production of low-mass polar molecules with radicals along with other thermal pyrolysis products. These aging heterogeneous could be activated as charge carriers and account for increase in the charge density (n) which increases conductivity (σ) and eventually leakage current density (J) according to the relationship in Equations (5) and (6). In conclusion, it is worthy to say that the dielectric properties of PI including the relative permittivity and leakage current density is deteriorated as a result of thermal aging process.

The variation of AC breakdown strength of PI over different aging durations (0–170 h) is highlighted in Figure 34d. The breakdown strength of PI shows a decreasing trend with aging progress (0–170 h). A noticeable reduction in breakdown strength can be seen at the later stage of aging process (120–170 h). The decline in breakdown strength of PI is attributed to the formation of low-mass polar molecules due to oxidation and degradation of the PI polymer structure which increases electrical conductivity. Moisture ingression in PI due to aging also plays a role in diminishing the breakdown strength of PI. Overall, dielectric integrity of PI is compromised due to aging process making PI more susceptible to electrical breakdown.

4 | Conclusions

Thermal aging was performed in presence of air and humidity and resultant change in properties (morphology, optical, thermal, dielectric, and mechanical properties) of PEEK, PTFE, and PI were thoroughly investigated. The results indicate a progressive increase in hardness and brittleness of PEEK, attributed to aging-induced structural transformations. Surface and bulk morphology analysis of PEEK revealed increased roughness, diminished surface gloss, and enhanced carbonization. The thermal decomposition temperature decreased, indicating thermal degradation, while the reduction in crystallinity suggests molecular rearrangement under oxidative conditions. Mechanical analysis of PEEK demonstrated an increase in

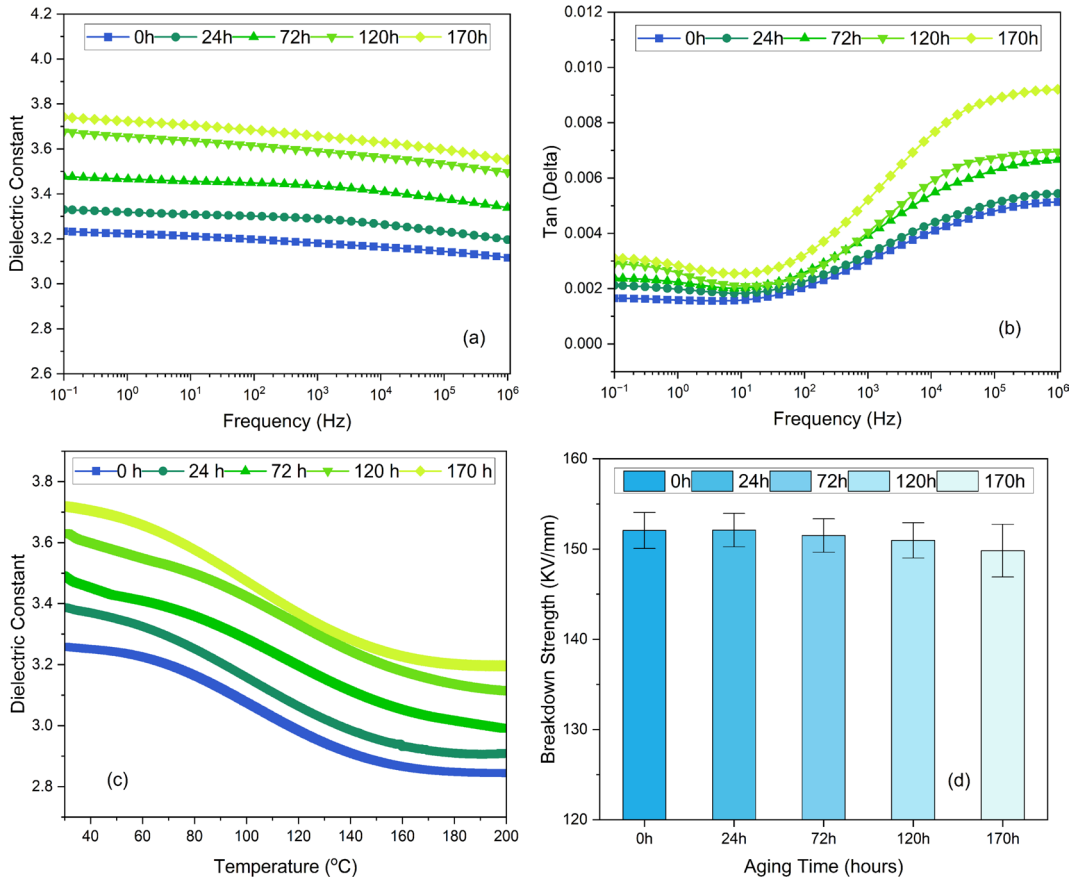

FIGURE 34 | Dielectric properties of PI samples with aging time: (a) dielectric constant, (b) dielectric loss, (c) dielectric constant versus temperature, and (d) AC breakdown strength. [Color figure can be viewed at wileyonlinelibrary.com]

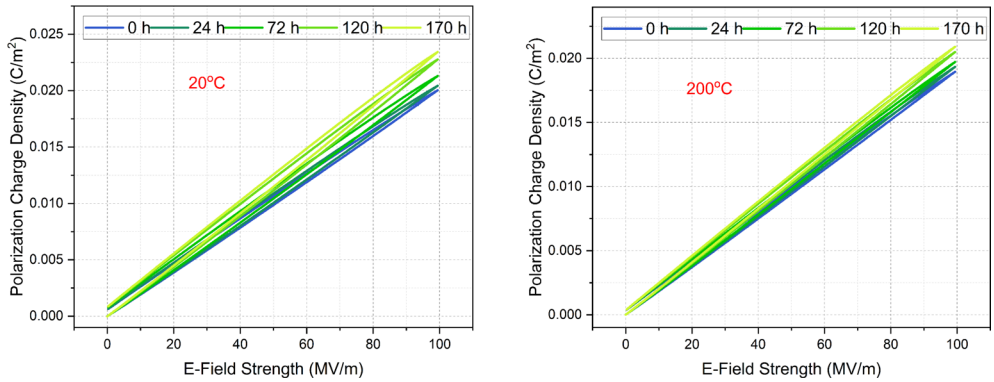

FIGURE 35 | Polarization of PI samples with aging time at room temperature and 200°C. [Color figure can be viewed at wileyonlinelibrary.com]

tensile strength and storage modulus with aging extension due to solidification and crosslinking phenomena, accompanied by a decrease in elongation at break and a reduction in tan δ from DMA. Dielectric characterization of PEEK showed a decline in dielectric constant, polarization charge density, and leakage current after aging, likely due to the crosslinking mechanism in PEEK that limits molecular mobility.

In case of PTFE, the tensile strength and elongation at break decreased after aging, indicating mechanical degradation and embrittlement. Microscopic analysis of PTFE revealed surface oxidation, discoloration, and signs of deterioration, suggesting oxidative degradation mechanisms. Thermal decomposition temperature remained largely unchanged for PTFE. The dielectric analysis showed a reduction in electronic polarization of PTFE with aging progress due to chain scission, which increased free volume and disrupted charge storage capability. Additionally, leakage current density of PTFE increased with aging time due to the formation of electronic localized states that facilitated charge carrier motion. The storage modulus of PTFE decreased, while the loss tangent increased with aging progress, reflecting a decline in mechanical stability of PTFE with aging. AC breakdown strength exhibited a slight reduction after aging, further confirming degradation in dielectric performance of PTFE.

For PI, aging resulted in severe mechanical degradation, with tensile strength decreasing by 54% and elongation reducing by 16%. Microstructure morphology revealed microvoids and surface defects reflecting oxidation of aromatic rings which also led to noticeable darkening of the PI films. During the aging process, PI absorbed moisture, facilitating the generation of low-mass polar molecules, which contributed to the degradation of its dielectric properties. This was evidenced by an increase in dielectric permittivity, polarization, and leakage current density, along with a reduction in AC breakdown strength. These findings offer valuable insights for future engineering applications. Future work will focus on long-term aging studies incorporating cold temperature effects to better replicate real-world service conditions in aerospace applications.

Author Contributions

Jawad Ahmad: data curation (lead), formal analysis (lead), investigation (lead), methodology (lead), writing – original draft (lead). **Mohamad Ghaffarian Niasar:** funding acquisition (lead), project administration (lead), writing – review and editing (supporting).

Acknowledgments

This project is funded by the Dutch Nationaal Groeifonds (NGF) program Luchtvaart in Transitie, project STD1 Elektrische Kabelsystemen (Grant No. 31194660), which is gratefully acknowledged.

Conflicts of Interest

The authors declare no conflicts of interest.

Data Availability Statement

The data available upon request from authors.

References

1. M. Borghei and M. Ghassemi, "Insulation Materials and Systems for More- and all-Electric Aircraft: A Review Identifying Challenges and Future Research Needs," *IEEE Transactions on Transportation Electrification* 7 (2021): 1930–1953, https://doi.org/10.1109/tte.2021.3050269.

2. "*ASD-STAN*" – Aerospace Series Cable Code Identification List.

3. J. H. Collins, "The Challenges Facing U.S. Navy Aircraft Electrical Wiring Systems," in *9th Joint FAA/DoD/NASA Aging Aircraft Conference* (2006), 11.

4. S. Ebnesajjad, *Fluoroplastics, Volume 2: Melt Processible Fluoropolymers. The Definitive User's Guide and Databook (Plastics Design Library)* (William Andrew Publishing, 2015), 9.

5. M. Bauccio, *ASM Engineering Materials Reference* (ASM International, 1994), 392.

6. *PTFE Insulated Terminals, Technical Data* (Farnell Co., 2010), http://www.farnell.com/datasheets/8067.pdf.

7. J. Shackelford and W. Alexander, *CRC Materials Science and Engineering Handbook* (CRC Press, 1992), 742.

8. B. Riddle and J. Baker-Jarvis, "Complex Permittivity Measurements of Common Plastics Over Variable Temperatures," *IEEE Transactions on Microwave Theory and Techniques* 51 (2003): 727–733.

9. G. Lopez, "High-Performance Polymers for Aeronautic Wires Insulation: Current Uses and Future Prospects," *Recent Progress in Materials* 3, no. 1 (2021): 005, https://doi.org/10.21926/rpm.2101005.

10. G. Skirbutis, A. Dzingutė, V. Masiliūnaitė, G. Šulcaitė, and J. Žilinskas, "A Review of PEEK Polymer's Properties and Its Use in Prosthodontics," *Stomatologija* 19, no. 1 (2017): 19–23.

11. T. Onodera, J. Nunoshige, K. Kawasaki, K. Adachi, K. Kurihara, and M. Kubo, "Structure and Function of Transfer Film Formed From PTFE/PEEK Polymer Blend," *Journal of Physical Chemistry C* 121, no. 27 (2017): 14589–14596.

12. M. Zalaznik, M. Kalin, and S. Novak, "Influence of the Processing Temperature on the Tribological and Mechanical Properties of Poly-Ether-Ether-Ketone (PEEK) Polymer," *Tribology International* 94 (2016): 92–97.

13. M. Younis, A. Unkovskiy, A. ElAyouti, J. Geis-Gerstorfer, and S. Spintzyk, "The Effect of Various Plasma Gases on the Shear Bond Strength Between Unfilled Polyetheretherketone (PEEK) and Veneering Composite Following Artificial Aging," *Materials* 12, no. 9 (2019): 1447.

14. C. Zhu, H. Zhang, and J. Li, "Thermal Aging Study of PEEK for Nuclear Power Plant Containment Dome," *Journal of Polymer Research* 29 (2022): 5, https://doi.org/10.1007/s10965-021-02839-w.

15. T. Hou and H. Chen, "Isothermal Physical Aging of PEEK and PPS Investigated by Fractional Maxwell Model," *Polymer* 53, no. 12 (2012): 2509–2518.

16. V. Capodanno, E. Petrillo, G. Romano, R. Russo, and V. Vittoria, "Effect of Physical Aging on the Properties of Films of Amorphous Poly (Ether Ether Ketone) (PEEK)," *Journal of Applied Polymer Science* 65, no. 13 (1997): 2635–2641.

17. D. Li, S. Xu, and J. Li, "Effect of Thermal Oxygen Aging on the Crystallization and Insulation Properties of Polyether Ether Ketone," *Journal of Applied Polymer Science* 140, no. 16 (2023): e53745.

18. X. Huang, J. Martinez-Vega, and D. Malec, "Dielectric Breakdown and Morphological Evolution of PTFE During Thermal-Oxidative Ageing at Temperatures Lower and Higher Than the Melting Temperature," in *2013 Annual Report Conference on Electrical Insulation and Dielectric Phenomena* (IEEE, 2013), 148–151, https://doi.org/10.1109/CEIDP.2013.6748189.

19. S. W. Li, N. Wang, J. F. Guo, et al., "Effect of Thermal Ageing on Electrical and Mechanical Properties of Tubular Bus Model Insulation," in *2016 IEEE International Conference on High Voltage Engineering and Application (ICHVE)* (IEEE, 2016), 1–4, https://doi.org/10.1109/ICHVE.2016.7800723.

20. M. Nagao, G. Sawa, and M. Ieda, "Dielectric Breakdown of Polyimide Film in High-Temperature Region," *Electrical Engineering in Japan* 97, no. 3 (1977): 7e11.

21. A. N. Hammoud, E. D. Baumann, E. Overton, et al., "High Temperature Dielectric Properties of Apical, Kapton, Peek, Teflon AF, and Upilex Polymers," in *1992 Conference on Electrical Insulation and Dielectric Phenomena*, NASA Technical Memorandum 105753 (IEEE, 1992), 8.

22. S. Diaham, S. Zelmat, M. L. Locatelli, S. Dinculescu, M. Decup, and T. Lebey, "Dielectric Breakdown of Polyimide Films: Area, Thickness and Temperature Dependence," *IEEE Transactions on Dielectrics and Electrical Insulation* 17, no. 1 (2010): 18–e27.

23. S. Z. Li, R. S. Chen, and S. G. Greenbaum, "NMR Studies of Water in Polyimide Films," *Journal of Polymer Science Part B: Polymer Physics* 33, no. 3 (1995): 403–409.

24. J. Seo, A. Lee, J. Oh, and H. Han, "Effects of Diamines (1,4-Phenylene Diamine and 4,4′-Oxydianiline) on Water Sorption Behavior of Polyimide Thin Film," *Polymer Journal* 32, no. 7 (2000): 583–588.

25. J. Seo and H. Han, "Water Diffusion Studies in Polyimide Thin Films," *Journal of Applied Polymer Science* 82, no. 3 (2001): 731–737.

26. S. Niyogi, S. Maiti, and B. Adhikari, "Chemical Durability of Polyimide Blend Films," *Polymer Degradation and Stability* 68, no. 3 (2000): 459–464.

27. L. Calabrese, D. Palamara, P. Bruzzaniti, and E. Proverbio, "Assessment of High Performance SAPO-34/S-PEEK Composite Coatings for Adsorption Heat Pumps," *Journal of Applied Polymer Science* 138 (2021): e50076, https://doi.org/10.1002/app.50076.

28. C. Lu, S. Qiu, X. Lu, et al., "Enhancing the Interfacial Strength of Carbon Fiber/Poly(Ether Ether Ketone) Hybrid Composites by Plasma Treatments," *Polymers* 11, no. 5 (2019): 753, https://doi.org/10.3390/polym11050753.

29. J. M. Chalmers, W. F. Gaskin, and M. W. Mackenzie, "Crystallinity in Poly(Aryl-Etherketone) Plaques Studied by Multiple Internal Reflection Spectroscopy," *Polymer Bulletin* 11 (1984): 433–435, https://doi.org/10.1007/BF00265483.

30. A. Jonas, R. Legras, and J.-P. Issi, "Differential Scanning Calorimetry and Infra-Red Crystallinity Determinations of Poly(Aryl Ether Ether Ketone)," *Polymer* 32, no. 18 (1991): 3364–3370, https://doi.org/10.1016/0032-3861(91)90540-Y.

31. A. Pascual, M. Toma, P. Tsotra, and M. C. Grob, "On the Stability of PEEK for Short Processing Cycles at High Temperatures and Oxygen-Containing Atmosphere," *Polymer Degradation and Stability* 165 (2019): 161–169, https://doi.org/10.1016/j.polymdegradstab.2019.04.025.

32. A. G. Al Lafi, "FTIR Spectroscopic Analysis of Ion Irradiated Poly (Ether Ether Ketone)," *Polymer Degradation and Stability* 105 (2014): 122–133, https://doi.org/10.1016/j.polymdegradstab.2014.04.005.

33. B. Cheng, H. Duan, Q. Chen, et al., "Effect of Laser Treatment on the Tribological Performance of Polyetheretherketone (PEEK) Under Seawater Lubrication," *Applied Surface Science* 566 (2021): 150668, https://doi.org/10.1016/j.apsusc.2021.150668.

34. G. Dimitrios, C. Angeliki, W. Chris, M. W. Paul, and K. Mihalis, "A Multi-Technique and Multi-Scale Analysis of the Thermal Degradation of PEEK in Laser Heating," *Polymer Degradation and Stability* 211 (2023): 110282, https://doi.org/10.1016/j.polymdegradstab.2023.110282.

35. E. Courvoisier, Y. Bicaba, and X. Colin, "Multi-Scale and Multi-Technique Analysis of the Thermal Degradation of Poly (Ether Ether Ketone)," *Polymer Degradation and Stability* 51 (2018): 65–76, https://doi.org/10.1016/j.polymdegradstab.2018.03.001.

36. S. Z. D. Cheng, Z. Q. Wu, and B. Wunderlich, "Glass Transition and Melting Behavior of Poly (Thio-1,4-Phenylene)," *Macromolecules* 20, no. 11 (1987): 2802–2810.

37. E. J. Stober, J. C. Seferis, and J. D. Keenan, "Characterization and Exposure of Poly(Ether–Ether–Ketone) to Fluid Environments," *Polymer* 23 (1984): 1845–1852.

38. S. Kumar, T. Rath, R. N. Mahaling, et al., "Study on Mechanical, Morphological and Electrical Properties of Carbon Nanofiber/Polyetherimide Composites," *Materials Science and Engineering B* 141, no. 1–2 (2007): 61–70.

39. A. Dorigato, Y. Dzenis, and A. Pegoretti, "Nanofiller Aggregation as Reinforcing Mechanism in Nanocomposites," *Procedia Engineering* 10 (2011): 894–899.

40. S. G. Kuzak and A. Shanmugam, "Dynamic Mechanical Analysis of Fiber-Reinforced Phenolics," *Journal of Applied Polymer Science* 73, no. 5 (1999): 649–658.

41. O. A. Lambri, F. G. Bonifacich, J. Á. García, et al., "Mechanical Energy Losses in Commercial Crosslinked Low-Density Polyethylene in the Temperature Range Between 200 and 400 K," *Journal of Applied Polymer Science* 136 (2019): 47605, https://doi.org/10.1002/app.47605.

42. M. Schmid, A. Amado, and K. Wegener, "Materials Perspective of Polymers for Additive Manufacturing With Selective Laser Sintering," *Journal of Materials Research* 29, no. 17 (2014): 1824–1832.

43. R. H. Ding, L. Xu, and J. X. Li, "Investigation and Life Expectancy Prediction on Poly(Ether-Ether-Ketone) Cables for Thermo-Oxidative Aging in Containment Dome of Nuclear Power Plant," *Polymer Testing* 103 (2021): 107362.

44. S. Rhee and J. L. White, "Crystalline Structure and Morphology of Biaxially Oriented Polyamide-11 Films," *Journal of Polymer Science Part B: Polymer Physics* 40 (2002): 2624–2640.

45. J. Liu, L. Shen, H. Lin, Z. Huang, H. Hong, and C. Chen, "Preparation of Ni@UiO-66 Incorporated Polyethersulfone (PES) Membrane by Magnetic Field Assisted Strategy to Improve Permeability and Photocatalytic Self-Cleaning Ability," *Journal of Colloid and Interface Science* 618 (2022): 483–495.

46. I. M. Salin and J. C. Seferis, "Kinetic Analysis of High-Resolution TGA Variable Heating Rate Data," *Journal of Applied Polymer Science* 47, no. 5 (1993): 847–856.

47. N. Khare, P. K. Limaye, N. L. Soni, and R. J. Patel, "Gamma Irradiation Effects on Thermal, Physical and Tribological Properties of PEEK Under Water Lubricated Conditions," *Wear* 342 (2015): 85–91.

48. Y. Liuqing, O. Yoshimichi, H. Naoshi, and H. Shugo, "Aging of Poly(Ether Ether Ketone) by Heat and Gamma Rays – Its Degradation Mechanism and Effects on Mechanical, Dielectric and Thermal Properties," *Polymer Degradation and Stability* 142 (2017): 117–128, https://doi.org/10.1016/j.polymdegradstab.2017.06.002.

49. Y. Zhou, R. Han, X. Zhang, Y. Mao, X. Li, and B. Zhai, "Broadband Dielectric Characteristics of PEEK Material Used for Packaging Press Pack IGBT Devices," in *2020 4th International Conference on HVDC (HVDC)* (IEEE, 2020), 8–13, https://doi.org/10.1109/HVDC50696.2020.9292700.

50. F. Krener and A. Schonhals, *Broadband Dielectric Spectroscopy* (Springer, 2003).

51. M. Ritamaki, *Effect of Thermal Aging on Polymer Thin Film Insulations for Capacitor Applications* (Tampere University of Technology, 2014).

52. M. Kozako, N. Fuse, Y. Ohki, T. Okamoto, and T. Tanaka, "Surface Degradation of Polyamide Nanocomposites Caused by Partial Discharge Using IEC (b) Electrodes," *IEEE Transactions on Dielectrics and Electrical Insulation* 11, no. 5 (2004): 833–e839.

53. M. Miyamoto, N. Tomite, and Y. Ohki, "Comparison of Gamma-Ray Resistance Between Dicyclo-Pentadiene Resin and Epoxy Resin," *IEEE Transactions on Dielectrics and Electrical Insulation* 23, no. 4 (2016): 2270–e2277.

54. Q. Fan, L. Lian, T. Guanyu, et al., "Effect of Thermal Oxidative Ageing on the Molecular Structure and Tribological Properties of Polytetrafluoroethylene," *Tribology International* 188 (2023): 108850, https://doi.org/10.1016/j.triboint.2023.108850.

55. I. S. Perelygin, M. Z. Peskova, Z. Z. Zakirov, and I. M. Glikin, "Determination of the Crystallinity of Polytetrafluoroethylene From Infrared Absorption Spectra," *Journal of Applied Spectroscopy* 24 (1976): 732–734.

56. X. Huang, J. Martinez-Vega, and D. Malec, "Morphological Evolution of Polytetrafluoroethylene (PTFE) During Thermal-Oxidative Ageing Above and Below the Melting Temperature," in *2013 IEEE International Conference on Solid Dielectrics (ICSD)* (IEEE, 2013), 628–631, https://doi.org/10.1109/ICSD.2013.6619846.

57. M. Mohammadian-Kohol, M. Asgari, and H. R. Shakur, "Effect of Gamma Irradiation on the Structural, Mechanical and Optical Properties of Polytetrafluoroethylene Sheet," *Radiation Physics and Chemistry* 145 (2018): 11–18, https://doi.org/10.1016/j.radphyschem.2017.12.007.

58. Q. Liu, J. Li, C. Cong, et al., "Thermal and Thermo-Oxidative Degradation of Tetrafluoroethylene–Propylene Elastomer Above 300°C," *Polymer Degradation and Stability* 177 (2020): 109180, https://doi.org/10.1016/j.polymdegradstab.2020.109180.

59. G. Wu, J. Gu, and X. Zhao, "Preparation and Dynamic Mechanical Properties of Polyurethane-Modified Epoxy Composites Filled With Functionalized Fly Ash Particulates," *Journal of Applied Polymer Science* 105, no. 3 (2007): 1118–1126.

60. M. A. Ibrahim, H. Çamur, M. A. Savaş, et al., "Dynamic Mechanical Thermal Analysis of PTFE Based Composites," *AIP Conference Proceedings* 2643, no. 1 (2023): 050019, https://doi.org/10.1063/5.0110479.

61. C. M. Simon and W. Kaminsky, "Chemical Recycling of Polytetrafluoroethylene by Pyrolysis," *Polymer Degradation and Stability* 62, no. 1 (1998): 1–7.

62. C. Sun, "The Polarizing Properties of the Dielectrics Affected by the Electrostatic Field," *Physics and Engineering* 13, no. 3 (2003): 27–31.

63. R. A. Dine-Hart, D. B. Parker, and W. W. Wright, "Oxidative Degradation of a Polyimide Film: I. Initial Studies," *British Polymer Journal* 3 (1971): 222–225.

64. M. Tsukiji, W. Bitoh, and J. Enomoto, "Thermal Degradation and Endurance of Polyimide Films," in *IEEE International Symposium on Electrical Insulation* (IEEE, 1990), 88–91, https://doi.org/10.1109/ELINSL.1990.109715.

65. L. Zhang, Y. Zhou, Y. Mo, et al., "Dielectric Property and Charge Evolution Behavior in Thermally Aged Polyimide Films," *Polymer Degradation and Stability* 156 (2018): 292–300, https://doi.org/10.1016/j.polymdegradstab.2018.06.009.

66. B. K. P. Scaife, *Principles of Dielectrics* (Clarendon Press, 1989).

67. J. O. Simpson and A. K. St Clair, "Fundamental Insight on Developing Low Dielectric Constant Polyimides," *Thin Solid Films* 308–309 (1997): 480–e485.

68. R. Torrecillas, A. Baudry, J. Dufay, and B. Mortaigne, "Thermal Degradation of High Performance Polymers – Influence of Structure on Polyimide Thermostability," *Polymer Degradation and Stability* 54, no. 2–3 (1996): 267–e274.

69. R. M. A. A. Majeed, A. Datar, S. V. Bhoraskar, P. S. Alegaonkar, and V. N. Bhoraskar, "Dielectric Constant and Surface Morphology of the Elemental Difussed Polyimide," *Journal of Physics D: Applied Physics* 39 (2006): 4855–4859.